Modelling of Heat and Mass Transfer Mechanisms in the Iron Ore Sintering Process

Joel A. Samsu, BSc

Ao.Univ.-Prof. Dipl.-Ing. Dr.techn. Christian Weiß
Chair of Process Technology and Industrial Environmental Protection
University of Leoben

A thesis submitted for the degree of
Master of Science

Leoben, November 2014

Affidavit

I declare in lieu of oath, that I wrote this thesis and performed the associated research myself, using only literature cited in this volume.

Eidesstattliche Erklärung

Ich erkläre an Eides statt, dass ich die vorliegende Masterarbeit selbständig und ohne fremde Hilfe verfasst, andere als die angegebenen Quellen und Hilfsmittel nicht benutzt und die den benutzten Quellen wörtlich und inhaltlich entnommenen Stellen als solche erkenntlich gemacht habe.

November 2014 Joel A. Samsu

Acknowledgements

I would like to extend my gratitude to my supervisor, Christian Weiß, for his guidance in writing this master's thesis. It has been a very valuable learning process for me.

I would also like to thank my wife, Anung, and my family for their support during my studies and the process of completing this work.

Abstract

The iron ore sintering process is one of the most important pre-treatment steps in integrated steel plants. Research around the world aims at a better understanding of the involved mechanisms in order to produce high quality burden for the steel making process. This work studies mechanisms of heat and mass transfer as well as the chemical reactions in the sintering process by setting up numerical case studies with the finite element software COMSOL Multiphysics®. The sintering bed is described by a multigeometry approach that involves a separate treatment of the solid and fluid domain and facilitates exchange between the two domains through coupling of the temperatures and chemical species concentrations. The heterogeneous reactions have been modelled as surface reactions at the gas/solid interface. The resulting temperature and concentration profiles have been discussed extensively regarding the applicability of the software and the employed methods respectively. The case studies calculated the heat transfer between the gas and solid phase and showed the travelling of the heat front in the sintering bed. In another model the gas phase reactions and their reaction rates were implemented resulting in the concentration profiles of the chemical species in the bed. The heterogenous surface reaction was coupled with the heat and mass transfer in the bed. The integration of submodels involved in an overall description of the iron ore sintering process still need to be further developed in order to create a comprehensive process model.

Kurzfassung

Der Sinterprozess stellt einen der wichtigsten Vorbehandlungsschritte in der Eisen und Stahlerzeugung im Rahmen der Hochofenroute dar. Zahlreiche Forschungseinrichtungen weltweit beschäftigen sich mit der Erforschung der Grundmechanismen zur besseren Beherrschbarkeit der Herstellungsprozesse und in der Folge zur Produktion von hochqualitativem Sinter für den Einsatz in der Stahlherstellung. Diese Arbeit beschäftigt sich mit der numerischen Simulation von Fallbeispielen zur Untersuchung der grundlegenden Mechanismen des Wärme- und Stofftransports sowie der chemischen Reaktionen im Sinterprozess. Die vorliegenden Beispiele wurden mit der finiten Elemente Software COMSOL Multiphysics® erstellt. Dabei wurde ein sogenannter „multigeometry approach" angewandt der das Sinterbett in zwei Gebiete teilt, diese separat berechnet und durch Kopplung der beiden Gebiete die Gleichungen für die Wärme- und Stoffaustauschprozesse löst. Die resultienden Temperatur- und Konzentrationsverläufe wurden hinsichtlich der Anwendbarkeit der Software und angewandten Methoden untersucht. In den Fallbeispielen konnte der Wärmeaustausch zwischen Feststoff und Gasphase und das Fortschreiten der Temperatur innerhalb des Sinterbettes modelliert werden. Ebenfalls konnten die Reaktionen in der Gasphase inklusive deren Reaktionraten implentiert und die Konzentrationsverläufe der einzelnen Spezies im Bett dargestellt werden. In einem weiteren Modell wurde die heterogene Reaktion von Sauerstoff und Kohlenstoff als Oberflächenreaktion berechnet und mit dem Wärme- und Stofftransport gekoppelt. Eine Integration der einzelnen Submodelle und Ergänzungen zu den bereits getesteten Fallbeispielen sind notwendig auf dem Weg zu einem vollständigen Modell des Sinterprozesses.

Contents

Chapter 1

Introduction

In the beginning of the 20^{th} century iron ore sintering was introduced as a way to reuse revert material from the blast furnace by fusing iron ore fines and dust from off-gas into larger particles [1]. Nowadays sintering is one of the most important pre-treatment steps in integrated steel plants, and research around the world aims at a better understanding of the involved mechanisms in order to produce high quality burden for the steel making process.

In this work certain aspects of the heat and mass transfer processes that occur during iron ore sintering will be modelled numerically using the finite element software package COMSOL Multiphysics®. Through the increase in computing power multiphysics modelling which typically involves solving coupled systems of partial differential equations has gained popularity in recent years. The applicability of multiphysics simulation for the solution of the heat and mass transfer problems in iron ore sintering is the subject of this thesis.

The iron ore sintering process has been described by numerous studies and by the use of laboratory tests in detail [2–4]. However, findings from these works can still vary from industrial experiences. From preceding theoretical analysis it is known that for example calculated pressure loss in the bed based on simplified idealized correlations can vary by one order of magnitude compared to values obtained during sinter production. By studying the transfer processes in the bed we aim to get one step closer to fully understand observed phenomena like the exemplary mentioned pressure loss.

In the context of this work it is relevant to know the characteristics of the processes involved in iron ore sintering. The following section gives an overview of the main steps of the iron ore sinter production, as well as the aspects of sintering productivity and sinter quality which are key parameters to asses the sintering process.

1.1 Iron Ore Sintering

The sintering process is part of the blast furnace route, the most common route in iron steel making [5]. Its purpose is the agglomeration of iron ore fines, which otherwise would be too small to be used in the blast furnace. The agglomeration is achieved through superficial melting of the fines, which after solidification stick together at their surfaces. The diameter of the considered particles ranges from 1 to 7 mm [6]. The whole process, from the raw material to the produced sinter cake, takes place in a sintering plant.

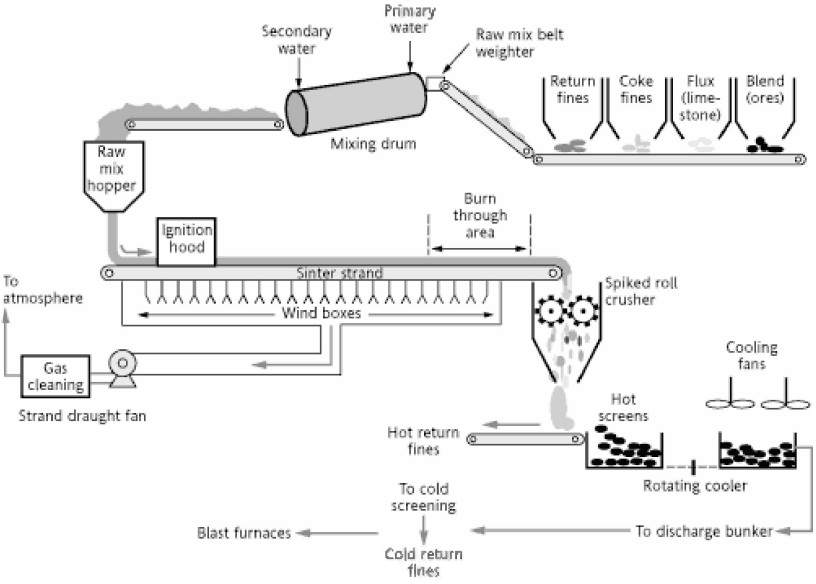

Figure 1.1: Schematic view of the sintering process [7].

A scheme of the sintering process is shown in Figure 1.1. In the first step the sinter blend is mixed according to a fixed composition of iron ore fines, fine coke breeze with particle diameters smaller than 3 mm, dolomite, limestone and recycled fine material from the sintering plant and dust from the plant's filters [6]. Subsequently water is added to the mix and the blend is granulated in a mixing drum. The processes of melting and solidification take place on a continuously moving conveyor, the sinter grate or „strand". After completed granulation the raw mix is delivered as a layer on the strand. At the beginning of the moving grate the cover layer is ignited with burners under the ignition hood. Dispersed fuel oil mixed with air at 4.5 bar is used as a fuel in the burners [6]. Alternatively coke oven gas, blast furnace gas and sometimes natural gas can also be used as fuels for ignition [7]. The sintering temperatures are in the range between 1200 and 1600°C [6]. For the heat transport from the surface through the bed and to ensure a „burn through" before the end of the strand, wind boxes are placed underneath the grate to suck

air through the sintering bed causing the coke to burn. The resulting waste gas is treated in a separate plant. After the sinter is discharged from the strand it is broken into pieces smaller than 200 mm and cooled down with air contact. Material smaller than 5 mm is recycled at the sintering plant.

1.1.1 Productivity and Sinter Quality

From a plant operators point of view the most important objective during the sintering process is to maximise the sinter output. However, it has to be considered that productivity impairs sinter quality up to a certain degree. In order to keep the desired balance between productivity and quality, detailed knowledge and understanding of the process properties is essential. The present study aims to improve understanding, prediction and control of the sintering process by modelling certain aspects of the heat and mass transfer processes in the sintering bed. Improvements in heat utilisation will result in first rate sinter and maximum productivity.

1.1.1.1 Sintering Productivity

The productivity of the iron ore sintering process is a simple and measurable performance indicator of a sintering plant. It is defined as the plants mass output of produced sinter per time. In order to be able to compare the productivity of different plants or the results from sinter pot tests, the productivity can be divided by the considered area of the strand or sinter pot respectively.

As already mentioned above a thorough movement of the flame front from the top to the bottom layer of the sinter mix needs to be ensured before the end of the strand. The flame front speed and the temperatures in the flame front are determined by the properties and efficiency of heat transfer in the sintering bed. In general it can be postulated that a more efficient heat transfer leads to a faster movement of the flame front and subsequently to a higher productivity. The increase in sintering productivity is based on the premise that the same amount of heat can be delivered with different intensities, e.g. by high temperatures over a short period of time or by low temperatures over a long period of time. The delivered heat is the same in both cases. Evidently these two extremes differ in productivity and quality of the output material.

1.1.1.2 Sinter Quality

One of the main issues concerning iron ore sinter quality is the sinter strength. A structurally stable sinter is necessary in order to utilize the sinter as feed material in the blast furnace. If the sinter is too fragile, it will be crushed under the load of the above layers in the blast

furnace, which would impair the gas flow and lead to a bad performance of the furnace. Another requirement for a good sinter is a certain minimal value of porosity to ensure gas permeability for ore reduction.

A strong sinter results from slow production at low maximum temperatures, which is contrary to the requirements for high productivity. This conflict makes it necessary to optimise the sintering process with respect to heat transfer. The porosity of the sinter is mainly dependent on granulation and properties of the raw sinter mix such as ore type, melt properties and fuel reactivity. The state of the art for optimizing and maintaining sinter quality and the usage of goethitic iron ore instead of haematite with all its implications for sintering productivity and sinter quality has been described and summarised in a review article by C. E. Loo [8].

1.2 Problem Statement

The descriptions in the previous section give an impression of the complexity of the process and the numerous factors that play a role in iron ore sinter production. The heat and mass transfer processes that are the subject of this work take place on the strand starting at ignition until "burn through" is established. During that timespan the layers of the sinter mix are transformed into the final product.

This work aims at describing key phenomena of the sintering process. The description of these phenomena leads to better understanding of the heat and mass transfer processes and of the parameters that influence sinter production. This however means that the thesis does not result in a complete numerical study of the sintering process as a whole.

Another motivation behind this work is to apply multiphysics simulation to study the interaction of heat and mass transfer as well as the chemical reactions occurring in the sintering bed. It will be possible to transfer the findings of this work to similar problems where transfer processes between gas and solid occur. An example for such applications are the heterogeneous gas phase reactions in a catalytic bed reactor.

The approach used to model heat and mass transfer in the bed is to set up case studies that examine the key phenomena of the sintering process. The methodology allows to study aspects of heat and mass transfer separately before coupling them in one case study.

Particular attention has been paid to the exchange processes between the gas in the bed and the solid particles. The bed has been modelled with a multigeometry approach (cf. Chapter 3) where two separate models for the fluid and the solid domain have been set up and coupled to account for the transport between the two domains.

Emphasis has also been placed on modelling the heterogeneous reactions which represent the combustion of coke in the bed. In the current literature no COMSOL models that

are suitable representations of heterogeneous combustion reactions have been found. The approach used in this study is to model the heterogeneous reaction as a surface reaction on spherical particles in a flow cell.

Chapters 2 and 3 are the basis for understanding the case study simulations. In Chapter 2, the fundamental heat and mass transfer mechanisms and their role in iron ore sintering will be explained. Chapter 3 describes the implementation of the model into the numerical simulation. Assumptions as well as the used model equations will be discussed in this chapter. The case studies that have been set up in order to study the transport phenomena in the bed are specified in Chapter 4. The model geometries, COMSOL interfaces, initial and boundary conditions and the meshing of the models will be explained for each particular case along with the ensuing implications. The obtained results will be presented and discussed in Chapter 5. A short summary and the drawn conclusions of this work are the subject of Chapter 6.

Chapter 2

Model Description

As the sinter mix moves from the starting point under the ignition hood to the drop off point at the end of the grate, heat transfer facilitates and maintains the process of transformation from the raw material called the "green mix" to the end product, the sintered cake. Prediction and control of the heat transfer and knowledge of the occurring reactions is essential for the industrial production of high quality sinter. In order to do so, the physical characteristics of the raw material, the treatment of heterogeneity in the model domain, the different terms of the heat and energy balances, as well as a detailed description of the heat transfer, chemical reactions and its implications for the sintering process will be the subject of this chapter.

2.1 Physical Description

The model domain considered in this study, i.e. the sinter mix where heat transfer and combustion take place, is structurally similar to a packed bed where the domain constitutes of an assembly of particles of different size and shape and the void space between the particles is the area where the gas can flow through the bed. This random structure of particles can be described with statistical methods, by assigning mean values to the parameters that describe the structure of the bed. This averaging makes the domain appear as if it would be a regular and consistent structure and thereby facilitates calculations.

The key parameters to describe the structure of a packed bed are the porosity or void fraction and the mean diameter of the particles in the bed [9]. The dimensionless porosity ε is defined as the volume of the void space divided by the total volume of the bed which by definition gives a value between 0 and 1. A value close to 0 describes a densely packed bed with very little void space, a value closer to 1 in contrast has lots of void space and is referred to being porous. As it is not always possible to measure the pore volume to calculate the

void fraction, it is also possible to determine the porosity by using Equation 2.1.

$$\varepsilon = 1 - \frac{\rho_{bulk}}{\rho_{particle}} \tag{2.1}$$

The bulk density ρ_{bulk} can be calculated by dividing the total mass of the structural material by the volume as a whole. The particle density $\rho_{particle}$ is a material property that can be taken from literature. Other methods to determine porosity include optical methods, CT scans or various intrusion techniques [10]. The porosity of a packed bed is dependent on the particle size, particle shape and the arrangement of the particles in the bed. To meet desired bed properties, e.g. permeability and stability of the bed, the porosity may be altered by compression, loosening or granulation of the raw material. Also mixing of small and large particles can lead to small porosity values. To emphasise this idea Table 2.1 lists exemplary porosity values of different materials. The table indicates the difficulty involved in the specification of porosity values as for some materials the undergone pretreatment needs to be considered and for some particle arrangements the porosity values can only be defined within a certain interval.

Material	Porosity ε [-]
densest packing of equal spheres	0.2595
quartz sand (loosend)	0.40
silica flour ($97\% < 40\mu m$)	0.61
corn (poured)	0.37
packing of a packed bed reactor	$0.60 - 0.95$
fluidised bed	$0.40 - 0.95$
filter cake	$0.50 - 0.90$

Table 2.1: Exemplary porosity values of different materials [10].

Descriptions of the size of non spherical particles in a bed are often done by ascribing an equivalent diameter, i.e. for example the diameter of a sphere with the same volume or surface area [11]. A frequently used diameter to describe transfer processes where active surface area is important is the Sauter mean diameter (SMD), which is defined as the diameter of a sphere that has the same volume to surface ratio as the particle ensemble of interest.

When gas flows through the bed, it faces resistance from the solid particles, which results in viscous and inertial energy losses and a pressure drop Δp. The pressure drop along the bed height H can be calculated with the Ergun equation (cf. Eq. 2.2) [12], which considers the superficial gas velocity u, the density and viscosity of the fluid (ρ_f and η_f) and the structure of the bed characterised by the particle diameter d_p and the bed porosity ε.

$$\frac{\Delta p}{H} = 150 \cdot \frac{(1-\varepsilon)^2}{\varepsilon^3} \cdot \frac{\eta_f \cdot u}{d_p^2} + 1.75 \cdot \frac{(1-\varepsilon)}{\varepsilon^3} \cdot \frac{\rho_f \cdot u^2}{d_p} \tag{2.2}$$

The first term on the right side of the equation represents the viscous flow and the second term is called the turbulent term. The proportionality constants for the two terms have been determined empirically. Although Ergun originally derived the equation for a bed with spherical particles and under usage of several assumptions, its results have proved suitability for many applications and is still widely used for calculating the pressure loss in porous structures. However, the model in this work does not consider pressure loss over the bed, but rather applies a uniform gas velocity for the whole simulation.

The porosity ε_b of the bed is a parameter to describe the macroscopic scale of the sinter mix. The microscopic scale on the other hand is described by the porous structure of a single particle (ε_p) and plays an important role when chemical reactions at the particle surface are governed by diffusion into the particle, but not for the heat transfer into the particle.

Handling the heat and mass transfer between the two phases is a challenging task, that demands a good physical model of the macro and micro structure. In this study the two levels are treated separately by setting up mass and energy balances for the fluid and the solid domain and simultaneously transfer mass and energy between these two domains. The fluid domain represents the gas that flows through the macro structure of the bed and transfers heat to the solid particles. The solid domain constitutes of the particles in the bed, where the heat from the gas is received and the combustion of coke takes place. At the same time the gaseous reactants diffuse into the particle oxidising the coke which releases heat that is again transferred back from the solid particles to the gas in the fluid domain. The set up of the mass and energy balances and the heat transfer mechanisms will be explained in the further sections of this chapter. The implementation into the model is the subject of Chapter 3.

2.2 Mass and Energy Balances

A first step when balancing any property in a system is to divide the system into smaller elements. By connecting simple element equations over many subdomains, a more complex equation over a larger domain can be approximated. A common approach in fluid dynamics is to divide the system into control volumes (cf. Fig. 2.1), and set up the equations for each volume by defining all the incoming and outgoing terms as well as the sinks and sources in the volumes [13].

The control volume in Figure 2.1 describes the balance of a one-dimensional model. The flow terms are only defined for the x-direction and can only enter and leave the volume on the left or right side of the square. Depending on the model the control volume can also be a square with flow terms in the x and y-direction or a cube where the terms are defined for

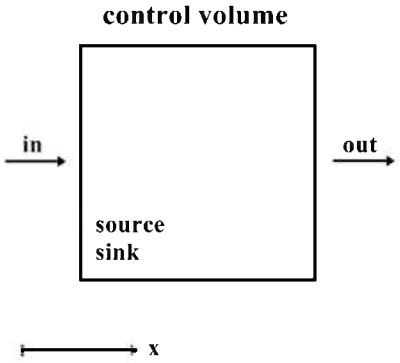

Figure 2.1: One-dimensional control volume approach for the set-up of mass and energy balances.

all three dimensions. The concept of the control volume is expressed by the simple notation for the balance of any property ϕ in Equation 2.3.

$$\frac{d\phi}{dt} = \dot{\phi}_{in} - \dot{\phi}_{out} + \dot{S}_{\phi} \tag{2.3}$$

The equation states that the rate of change of the property ϕ in the control volume (on the left hand side of the equation), is equal to the difference of the incoming and outgoing amount of ϕ, plus the generated or dissipated amount of ϕ, represented by the term $\dot{S}_{\phi}$, which is positive for a source and negative for a sink. The dots on the terms in the equation signify that the terms refer to a flux or rate with the specific unit of ϕ per unit time.

This scheme is the basis for mass and energy balances in chemical process engineering and is applied to balance heat and chemical species in chemical reactors. In the next section the fundamental conservation laws for the balances in the heat transfer model of the sintering process will be explained.

2.3 Conservation Equations

The foundation of every analysis of a certain property in a system are the conservation laws and balances of the studied properties. The different terms of the conservation equations need to be defined more specifically, to be able to calculate the change in temperature and the species concentration in the model. To account for the specific transfer mechanisms in the sintering process, the terms of the balance in Equation 2.3 need to be adapted and the control volume is scaled down infinitesimally, which leads to a set of differential equations for the conservation laws.

Here the concept of the conservation equations will be explained by looking at the general differential form of the conservation equation (Eq. 2.4) for any quantity ϕ [13]. The

partial differential equation (PDE) is written for the one-dimensional case, in Cartesian coordinates and tensor notation.

$$\frac{\partial}{\partial t} \cdot (\rho \cdot \phi) + \frac{\partial}{\partial x} \cdot (\rho \cdot u_x \cdot \phi) = \frac{\partial}{\partial x} \cdot (\Gamma \cdot \frac{\partial \phi}{\partial x}) + \dot{S}_\phi \tag{2.4}$$

The basic principle of the conservation equation is the same as for the control volume balance in Equation 2.3. The first term in both equations represents the rate of change for the considered quantity ϕ. The second and third term in the general form of the conservation equation describe different physical phenomena where the quantity is transferred inside the system. The last term in both equations is the source term for the quantity ϕ.

The variable ϕ in Equation 2.4 can be replaced depending on the considered quantity by 1 for the mass balance, by the fluid velocity u_x for the momentum equation and by the enthalpy h for the energy balance. The first term is called the transient term, which is 0 for stationary processes. The second term is the convective term, that describes the rate of change due to the movement of the fluid. The flux vector Γ is part of the diffusive term and is defined depending on the balanced quantity. It follows Fick's law for mass diffusivity of the particle motion, or Fourier's law for thermal diffusivity in heat transfer. The last term is defined depending on the nature of the problem. It has a positive value for the balance of any chemical species that is the product of a chemical reaction or for the heat balance if heat is generated in an exothermic reaction. It is negative for any reactant species or in the case of an endothermic reaction. In the following sections the special conservation laws for the mass, energy and species balances will be explained.

2.3.1 Conservation of Mass

The mass balance takes care of the fact that in a closed system mass can neither be destroyed or generated and therefore features one of the fundamental laws of fluid dynamics. The equation can be derived by application of the general form (Eq. 2.4) with $\phi = 1$. It is commonly called the continuity equation.

$$\frac{\partial \rho}{\partial t} + \frac{\partial}{\partial x}(\rho \cdot u_x) = 0 \tag{2.5}$$

The third and fourth term of the general form are 0. The equation states that, in a steady state process, the rate at which mass enters a system is equal to the rate at which it leaves the system.

2.3.2 Conservation of Energy

A simplified form of the energy conservation equation states that the rate of change of the internal energy in a system is equal to the difference of the in and outflowing energy (heat

and enthalpy), plus the energy of the heat sinks or sources. The variable ϕ in the general form is replaced by the specific enthalpy $h\,[J/kg]$.

$$\frac{\partial}{\partial t}(\rho \cdot h) + \frac{\partial}{\partial x}(\rho \cdot u_x \cdot h) = \frac{\partial}{\partial x}(\dot{q}_x) + Q \tag{2.6}$$

The enthalpy is the product of the specific heat capacity $c_p\,[\mathrm{J/(kg\,K)}]$ and the absolute temperature $T\,[K]$. The second term is the energy transported by the moving fluid and $\dot{q}_x\,[\mathrm{W/m^2}]$ is the heat flux in the x direction. The heat source term is represented by $Q\,[\mathrm{W/m^3}]$. The energy equation is the basis for implementing the heat transfer into the model of the sintering process.

2.3.3 Conservation of Species

The species conservation equation (Eq. 2.7) is derived in a similar way as the two equations above. In the first two terms $\rho\phi$ is replaced by the species concentration $c_i\,[\mathrm{mol/m^3}]$. The third term follows Fick's first law of molecular diffusion, with the diffusion coefficient $D\,[\mathrm{m^2/s}]$. The source term $R_i\,[\mathrm{mol/(m^3\,s)}]$ is the rate of production or consumption of the species i by the chemical reactions [14].

$$\frac{\partial c_i}{\partial t} + \frac{\partial}{\partial x} \cdot (u_x \cdot c_i) = D_i \cdot \frac{\partial^2 c_i}{\partial x^2} + R_i \tag{2.7}$$

Some of the terms may become zero or need further adjustment depending on the modelling assumptions and the fluid transport in the system. The source term in the species conservation equation is dependent on the kinetics of the chemical reactions.

In the following sections the heat transfer in the sintering process is explained by describing the fundamental heat transfer mechanisms and their implementation into the conservation laws.

2.4 Heat Transfer in Iron Ore Sintering

In the iron ore sintering process heat from ignition of the sinter mix top layer is transferred through the bed until it reaches the bottom layers of the bed. The movement of the high temperature zone is referred to as travelling of the flame front. The governing mechanisms as well as the different modes of heat transfer from and within the flame front have been described by C. E. Loo [2].

During the whole process the heat in the bed is transferred by conduction, convection and radiation. A simple one-dimensional scheme of the heat transfer from the flame front is shown in Figure 2.2. The transparent arrows signify that conduction and radiation act in both directions, i.e. up and downwards in the bed. Convection depicted by the bold grey

arrows acts only in the direction of the gas flow. Effectiveness of heat transfer will determine flame front speed and in consequence enhance sintering productivity [2]. Therefore a proper understanding of heat transfer in the sintering bed is very important. The following sections will describe the principles of conduction, convection and radiation and their role in iron ore sintering.

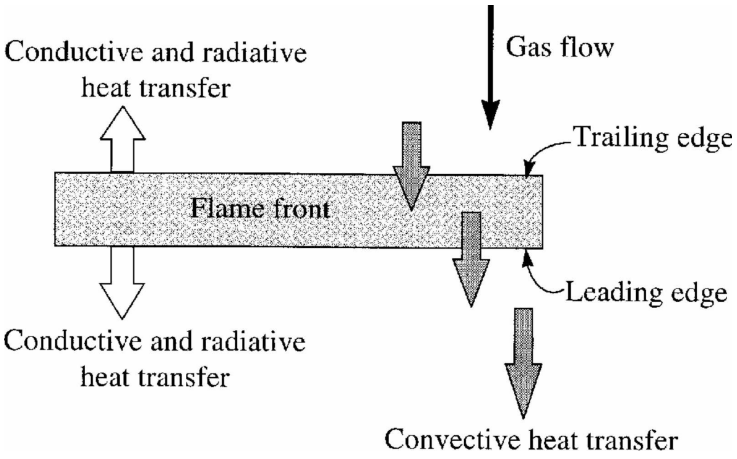

Figure 2.2: Schematic view of the heat transfer from the flame front [2].

2.4.1 Heat Transfer by Conduction

Heat transfer by conduction is the energy transfer between neighbouring molecules due to a temperature gradient in the observed material [15]. It is described by the empirical law of Fourier in Equation 2.8.

$$\dot{q} = -\lambda \cdot grad(T) \tag{2.8}$$

The heat flux density $\dot{q}$ [W/m^2] is the amount of energy transferred through a unit area per unit time. It is proportional to the thermal conductivity λ [W/(m K)] and the negative gradient of the temperature T. The thermal conductivity is a material property which is dependent on pressure and temperature. The negative sign for the temperature gradient is necessary to fulfil the 2$^{\text{nd}}$ law of thermodynamics which states that heat in a closed system travels from warm to cold temperatures [15]. The conductive heat transfer can be substituted into the diffusive term of the energy conservation equation (Eq. 2.6). The enthalpy is replaced by the product of the specific heat capacity $c_{p,p}$ and the temperature T_p of the particle.

In iron ore sintering conduction plays a dominant role within the flame front where the heat is transferred from the surface of the raw material to its cooler core in order to raise

the inner temperature of the solids [2]. The higher the value of the thermal conductivity, the faster is the heating process of the solid core. Another consequence of the conduction in the bed is the transfer of heat to adjacent particles in the sinter mix. Conduction also takes place in the moving gas, but plays only a minor role compared to the effect of convection.

2.4.2 Heat Transfer by Convection

In a flowing fluid, heat is transferred not only by conduction, but also by the macroscopic motion of the fluid, called the convective heat transfer [15]. It is represented by the second term of the energy conservation equation (cf. Eq. 2.6). To study the temperatures of the flowing gas in the bed, the enthalpy is replaced by the product of the specific heat capacity $c_{p,f}$ and the temperature T_f of the fluid.

A case of special interest is the convective transfer of heat between a moving fluid and a solid surface, e.g. a wall, or the surface of a pipe. In the case of the sintering process this is relevant for the heat transfer between the flowing gas and the particles in the bed. The convective heat transfer is calculated in Equation 2.9 and is defined as the heat flux density $\dot{q}$ [W/m^2] at the solid surface of the particle.

$$\dot{q} = \alpha \, (T_s - T_f) \tag{2.9}$$

The value of the heat transfer coefficient α [W/(m^2 K)], the proportionality factor used to calculate the convective heat transfer, is dependent on the temperature and velocity field of the fluid. A detailed description of the heat transfer coefficient calculation for the packed bed can be found in the Appendix. T_s is the surface temperature of the solid interface and T_f the "bulk temperature" of the fluid.

As conduction and radiation alone cannot raise high enough temperatures for a controlled burning of the coke particles in the bed, convective heat transfer is the main contributor to an effective and systematic downward movement of the flame front [2]. Convection causes the heat from conduction and radiation to move from regions above the flame front into the flame front. Similarly it causes heat to travel from the flame front to cooler regions ahead of it. It also enhances combustion of coke particles due to oxygen delivery through the bed.

2.4.3 Thermal Radiation

Thermal radiation is a form of electro-magnetic radiation which is emitted by all matter with a temperature greater than absolute zero [15]. Heat is transferred in form of electromagnetic

waves when the emitted energy of one object is absorbed by another object. The Stefan-Boltzmann Law (Eq. 2.10) describes the radiative energy emitted by one object.

$$\dot{q} = \epsilon \cdot \sigma \cdot T_s^4 \tag{2.10}$$

In this equation ϵ is the dimensionless emissivity of the object, which is smaller than 1 for any real object. The proportionality constant σ with a value of $5.67 \cdot 10^{-8}$ $[\mathrm{W/(m^2\,K^4)}]$ is called the Stefan-Boltzmann constant. The thermal radiation is proportional to the fourth power of the absolute temperature of the hot surface and therefore primarily gains importance with increasing temperatures.

As the temperatures in the flame front are at approximately 1600°C radiation plays a significant role within the flame front. It is usually treated in the source term of the energy equation.

2.5 Coke Combustion Mechanisms

The process of coke combustion delivers the amount of energy needed for the partial melting of the iron ore particles in the bed. Before the granulation the coke is added to the mix in form of coke breeze, which are coke particles with a diameter of less than 3 mm [6]. At the end of the sintering process, the major part of the coke in the bed has reacted with the air oxygen that has been sucked through the bed. In theory the coke combustion in the sintering bed can be described by the following set of reactions.

$$\mathrm{C(s) + O_2(g) \longrightarrow CO_2(g)} \tag{2.11}$$

$$\mathrm{C(s) + \tfrac{1}{2}\,O_2(g) \longrightarrow CO(g)} \tag{2.12}$$

$$\mathrm{CO(g) + \tfrac{1}{2}\,O_2(g) \longrightarrow CO_2(g)} \tag{2.13}$$

$$\mathrm{CO(g) + H_2O(g) \longleftrightarrow CO_2(g) + H_2(g)} \tag{2.14}$$

$$\mathrm{2\,CO(g) \longleftrightarrow C(s) + CO_2(g)} \tag{2.15}$$

Reactions 2.11 and 2.12 are the heterogeneous oxidation of the coke particles in the sintering bed. The second reaction is preferred over the first at temperatures higher than 1000°C and therefore Reaction 2.11 will be neglected in the model of the sintering process. Reactions 2.13 and 2.14, the homogeneous gas reactions, and the last reaction, Reaction 2.15 take place after the initial reaction of coke with oxygen depending on the kinetic parameters, species concentrations and temperature conditions in the sinter mix. The last reaction is called the Boudouard reaction and will be discussed in Section 2.5.3.

2.5.1 Heterogeneous Combustion Reaction

In the heterogeneous combustion reaction the coke particle is oxidised and carbon monoxide is the remaining product of the reaction. In the reaction model the combustion process progresses through the following 5 steps [14]:

1. The transport of oxygen from the bulk gas through the gas film to the particle surface
2. Diffusion of oxygen from the particle surface to the reaction interface
3. Coke combustion at the reaction interface
4. Diffusion of the reaction product (CO) from the reaction interface to the particle surface
5. Transport of CO from the particle surface to the bulk gas through the gas film

The gas film in step 1 (and step 5) is the boundary layer where the concentration of a chemical species is smaller than in the bulk gas. Similarly to the temperature boundary layer it is dependent on the properties of the flow field. The mass transfer coefficient β [m/s] is a measure for the species transport velocity through the boundary layer and shows many analogies to the heat transfer coefficient α. The calculations of the mass transfer coefficient are explained in the Appendix.

The diffusion step 2 (and step 4), the transport from the particle surface through its pores and to the reaction interface follows Fick's law of diffusion. The result of this process is a concentration gradient in the pores of the particles. The diffusion coefficient D_i [m^2/s] for the species i is dependent on diffusion regime and the porous structure, a circumstance that is accounted by defining an effective diffusion coefficient $D_{e,i}$. The effective diffusion coefficient is estimated by multiplying D_i with the void fraction available for the transport ε_t [–] divided by the tortuosity τ [–] (cf. Eq. 2.16 [16]). The values of the parameters that are needed in order to calculate effective diffusion coefficients are very difficult to obtain and often only empirical parameters are used.

$$D_{e,i} = D_i \cdot \frac{\varepsilon_t}{\tau} \tag{2.16}$$

The combustion reaction in step 3 is an exothermic reaction that leads to a decrease of the carbon concentration in the bed. The rate of combustion $R_{react,1}$ [kg/s] (cf. Eq. 2.17) is dependent on the surface temperature T_s of the reaction interface, the oxygen concentration c_{O_2} at the interface and the kinetic parameters of the combustion reaction (cf. Eq. 2.19). The heat of combustion Q [J/(m^3s)], adds as a source term in the energy equation and can be calculated by multiplying the reaction enthalpy H_r [J/mol] with the reaction rate

R_c [mol/(m^3 s)]. The standard reaction enthalpy for the combustion of carbon is equal to −110.5 kJ/mol [8].

Steps 4 and 5, the transport processes of the reactants from the reaction interface to the bulk phase are the reverse processes of steps 1 and 2. They basically underlie the same transport mechanisms as the first two steps. The combustion reaction at the interface leads to a change in the particle structure, i.e. a widening of the pore space and a decrease in density. The diffusion of the reactants from the reaction interface back to the bulk is quite fast and the last two steps are not regarded to be limiting the combustion reaction [18].

The limiting factor in the whole process of coke combustion can be found by analysing the above mentioned five steps. For example if the diffusion step is the slowest the heterogeneous reaction is called diffusion controlled. In order to improve the reaction rate in the sintering process a knowledge of the limiting steps is absolutely necessary.

In similar studies the coke combustion process has been described by the shrinking core model (cf. Fig. 2.3) [16]. In this model the heterogeneous reaction first takes place at the surface of the particle. After the reaction of carbon and oxygen, carbon monoxide leaves the particle and only ash is left at the surface of the particle where the carbon has reacted. Following this initial reaction step, the oxygen needs to diffuse through the ash layer to reach the underlying coke, in order for the oxidation reaction to continue. During the whole reaction the particle diameter stays constant and only the reacting core of coke in the the particle diminishes. At the end of this process the particle will still have the same size but will consist of inert material only and no reaction will take place any more.

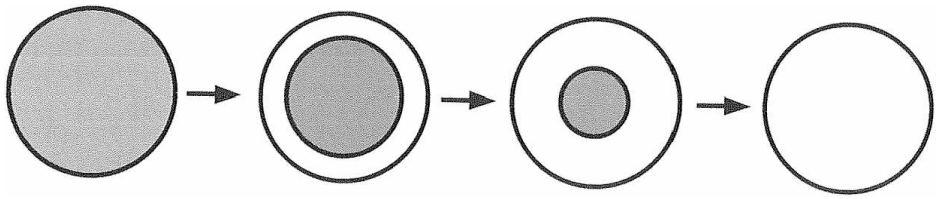

Figure 2.3: Shrinking core model describing a heterogeneous gas/solid reaction [19].

The total reaction rate of the coke combustion can be described by the following expression [20].

$$R_{react,1} = 2 \cdot \frac{M_C}{M_{O_2}} \cdot p_{O_2} \cdot k_{eff} \cdot A_p \tag{2.17}$$

M_C and M_{O2} are the molecular weight of carbon and oxygen, p_{O2} is the partial pressure of oxygen at the reaction interface and A_p is the surface area of the particle. The expression k_{eff} [s/m] denotes the effective reaction resistance and is dependent on the three steps in the

heterogeneous reaction model. The inverse of the effective reaction resistance is described by Equation 2.18.

$$\frac{1}{k_{eff}} = \frac{p_{O_2}}{\beta \cdot c_{O_2} \cdot M_{O_2}} + \frac{r_p^2 \cdot p_{O_2}}{r_c^2 \cdot k_s} + \frac{4\pi \cdot r_p \cdot (r_p - r_c) \cdot p_{O_2}}{D_{e,O_2} \cdot M_C \cdot c_{O_2} \cdot r_c} \tag{2.18}$$

The three terms on the right hand side of the equation describe the three steps for the whole reaction, i.e. the mass transfer through the gas film, the reaction kinetics and the diffusion to the reaction interface in the particle (from left to right). The mass transfer coefficient β influences the mass transport of the reactants to the particle surface and is dependent on the gas properties, the flow and temperature field, and can be calculated with the dimensionless Sherwood, Reynolds and Schmidt numbers (cf. Appendix). The mass transfer to the particle surface is also dependent on the oxygen partial pressure which is the product of the molar fraction of oxygen in the gas and the total pressure.

The second and third term in the reaction rate constant equation depend on the radius r_c of the reacting core which changes with respect to time. It decreasing as the mineral layer is increasing with the progress of the reaction. As a consequence also the surface of the reacting core decreases, which leads to a decrease of the reaction rate (cf. Eq. 2.17) and an overall slowdown of the combustion reaction.

The second term in Equation 2.18 includes the kinetic constant k_s [s Pa/m] of the heterogeneous combustion reaction which is a temperature dependent Arrhenius expression (cf. Eq. 2.19). The second term is also dependent on the particle and reacting core radii and again on the oxygen partial pressure at the reaction interface. The calculation from partial pressure to molar concentration units can be done by using the ideal gas law.

$$k_s = 860 \cdot \exp(-\frac{18000}{T_s}) \tag{2.19}$$

The third term in Equation 2.18 is dependent on the radii of the particle and the reactive core, partial pressure p_{O_2} of oxygen, the effective diffusion coefficient of oxygen in the pores, the molecular weight M_C of carbon and the local oxygen concentration c_{O_2}.

With the made assumptions the reaction rate can be calculated. At the beginning of the reaction the particle radius and the reacting core radius are the same and the expression $(r_p - r_c)$ is equal to zero. As a consequence the third term in Equation 2.18 is equal to zero and the reaction rate at the beginning depends on the first two terms only. These two terms include the oxygen concentration at the surface and in the sintering bed, the mass transfer coefficient β and the kinetic constant k_s. With the initial concentration change the following rate expressions can be calculated with respect to the change of the radius which can be calculated indirectly via the change in volume and mass of the reacting core due to the carbon oxidation reaction. The resulting reaction rate expression is decreasing with

time, as the radius and the surface of the reacting core are shrinking and the reaction will continue as long as the temperature and oxygen concentration are favouring the reaction.

2.5.2 Homogeneous Gas Reactions

The homogeneous reactions in the gas phase describe the oxidation of the main combustion product carbon monoxide with oxygen or water vapour forming carbon dioxide and hydrogen in the case of the water gas shift reaction (WGSR).

$$\mathrm{CO(g)} + \tfrac{1}{2}\,\mathrm{O_2(g)} \longrightarrow \mathrm{CO_2(g)}$$
$$\mathrm{CO(g)} + \mathrm{H_2O(g)} \longleftrightarrow \mathrm{CO_2(g)} + \mathrm{H_2(g)}$$

The reaction kinetics are temperature and concentration dependent Arrhenius expressions with the frequency factor k_i and the activation energy Ea_i as kinetic parameters. The oxidation with oxygen is a fast exothermic reaction and follows the rate expression in Eq. 2.5.2 [21]. The standard reaction enthalpy is $-283.0\,\mathrm{kJ/mol}$ [22] and the reaction kinetics are dependent on the concentrations of carbon monoxide, oxygen and water in the gas.

$$R_{react,2} = k_2 \cdot \exp(-\frac{Ea_2}{R \cdot T_f}) \cdot c_{CO} \cdot c_{O_2}^{\frac{1}{2}} \cdot c_{H_2O}^{\frac{1}{2}} \quad [\frac{mol}{m^3 s}] \tag{2.20}$$
$$k_2 = 1.3 \cdot 10^8 \quad [\frac{(m^3)^3}{mol^2 s}]$$
$$Ea_2 = 125604 \quad [\frac{J}{mol}]$$

The oxidation with water vapour in the gas phase of the sintering bed, also known as the water gas shift reaction, represents an equilibrium reaction described by the following kinetics [23].

$$R_{react,3} = k_3 \cdot (c_{CO} \cdot c_{H_2O} - \frac{c_{CO_2} \cdot c_{H_2}}{K_{eq}}) \quad [\frac{kmol}{m^3 s}] \tag{2.21}$$
$$k_3 = 2.78 \cdot 10^3 \cdot \exp(-\frac{1510}{T_f}) \quad [\frac{m^3}{kmol\ s}]$$
$$K_{eq} = 0.0265 \cdot \exp(\frac{3968}{T_f}) \quad [-]$$

The oxidation with water vapour is reversible and takes place at slower rates than the oxidation with oxygen. The reaction is kinetically favoured at high temperatures and thermodynamically favoured at low temperatures [24]. It is not affected by pressure, as the number of gas moles stays the same in both directions. The reaction is exothermic with a

standard reaction enthalpy of −41.09 kJ/mol [24]. The reaction rate equations contribute to the source terms of the species conservation equations and by multiplication with the corresponding reaction enthalpy also to the heat source term in the energy conservation equation.

2.5.3 Boudouard Reaction

The Boudouard reaction is a heterogeneous equilibrium reaction and is the oxidation of carbon with carbon dioxide forming two moles of carbon monoxide. The reaction in the reverse direction is the disproportionation of two moles of carbon monoxide, into CO_2 and carbon, which forms soot.

$$\mathrm{C(s) + CO_2(g) \longleftrightarrow 2\,CO(g)}$$

The reaction rate expression $R_{react,4}$ [kg/s] is given in Equation 2.22 [16]. The expression is identical to Eq. 2.17 for the coke combustion with oxygen but the definition of the effective reaction resistance k_{eff} [s/m] differs from the combustion reaction above.

$$R_{react,4} = 2 \cdot \frac{M_C}{M_{O_2}} \cdot p_{O_2} \cdot k_{eff} \cdot A_p \tag{2.22}$$

The inverse of k_{eff} is described by Equation 2.23. As for the heterogeneous combustion reaction this equation takes into account the diffusion of the reactants to the particle surface and into the particle to the reaction interface and the temperature dependence of the reaction which is a factor in the calculation of the kinetic constant k_s.

$$\frac{1}{k_{eff}} = \frac{p_{CO_2}}{\beta \cdot c_{CO_2} \cdot M_{CO_2}} + \frac{r_p^2 \cdot A_p}{r_c^2 \cdot k_s \cdot n_{CO_2} \cdot M_{CO_2}} + \frac{4\pi \cdot r_p \cdot (r_p - r_c) \cdot p_{CO_2}}{D_{e,CO_2} \cdot M_C \cdot c_{CO_2} \cdot r_c} \tag{2.23}$$

The calculation of the mass transfer coefficient β for the case of the sintering bed is described in the Appendix. All other parameters have already been explained for the combustion reaction. The kinetic constant k_s [s kg/m^3] of the Boudouard reaction is described by the following equation.

$$k_s = 63.3 \cdot \exp(-\frac{14051}{R \cdot T_s}) \cdot \frac{n_{CO_2} \cdot M_{CO_2}}{A_p} \tag{2.24}$$

The kinetic constant depends on the temperature at the surface T_s, the number of carbon dioxide molecules n_{CO_2} at the particle surface and the particle surface area A_p. The reaction in the forward direction is endothermic with a standard reaction enthalpy H_r of 159.7 kJ/mol [25] and therefore will be favoured at high temperatures. At low temperatures and high pressure, i.e. when the waste gas cools down, reversed direction will be favoured as it reduces the number of gaseous molecules.

Although the model of the coke combustion processes in the sintering bed only includes few chemical species the reaction system is quite complex and strongly depends on the transport processes, the temperature and species concentrations in the bed. The heat and mass transfer and the system of reactions which take part in the sintering process lead to a characteristic temperature profile that is a function of the time and the location in bed.

2.6 Temperature Profile in the Sintering Bed

The temperature profile in a sintering bed is the result of all occurring heat transfer mechanisms and the coke combustion described in the previous sections. It can be measured by implementing bed thermocouples into a lab-scale sinter pot. Such experiments allow the validation of numerical simulation results. The temperature profile can be expressed as a function of the sintering bed height at a certain time (cf. Fig. 2.4).

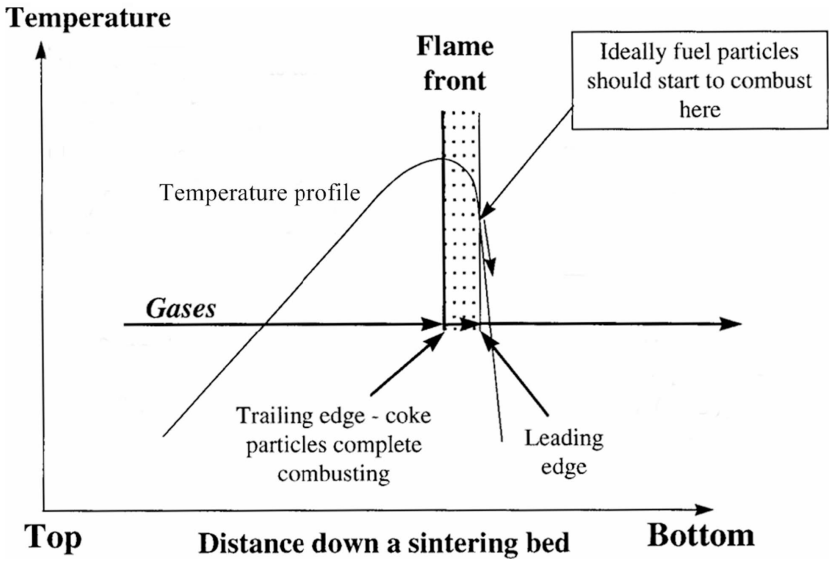

Figure 2.4: Temperature profile in the sintering bed as a function of the distance down the bed [2].

The left side in figure represents the top where the gas enters the sintering bed and the right side represents the bottom where the gas leaves the bed. The leading edge of the flame front is the zone where coke combustion starts and the trailing edge is signified by the place where a major part of the coke particles are fully consumed. The steep curve ahead of the flame occurs due to the instantaneous temperature increase caused by the reacting coke at combustion. The flowing gas that enters the bed at the top with ambient temperature

leads to a cooling of the bed. From the trailing edge upwards the temperature decreases at a steady rate.

Chapter 3

Numerical Implementation

The numerical modelling steps, including pre and post processing, solving of heat transfer and chemical reaction kinetics have been performed with the finite element program COMSOL Multiphysics®. In order to account for the transfer mechanisms in the fluid and solid phase of the sintering bed, a multi geometry model similar to the one used by Allain and Dixon [26] has been implemented.

3.1 Multi Geometry Modelling Approach

The transfer processes in a sintering bed can be compared to those occurring in a packed bed reactor. The packed bed reactor is one of the most common reactors in the chemical industry [27] and is used for heterogeneous gas/solid or fluid/solid reactions where heat and mass transfer processes between the solid and fluid phases occur.

A scheme of the pseudo-heterogeneous model used in this study is shown in Figure 3.1. The whole model consists of the packed bed containing the sinter mix and the fluid phase. The sinter mix in the bed is modelled as an assembly of monosized spherical particles. The fluid phase is described by a set of one-dimensional partial differential equations, accounting for the mass and energy balances in the fluid. The mass and energy transfer in the solid phase is also described by a set of one dimensional partial differential equations with r as the radial coordinate for the spherical formulation of the conservation equations. The particles are surrounded by the space and time dependent bulk temperature and bulk concentration of the fluid domain.

3.1.1 Fluid Domain Modelling

The fluid phase, i.e. the gas that flows through the sintering bed, is represented in a one-dimensional model where each coordinate represents a point along bed height H. Within the fluid phase, the heat transfer is governed by conduction and convection and the heat balance

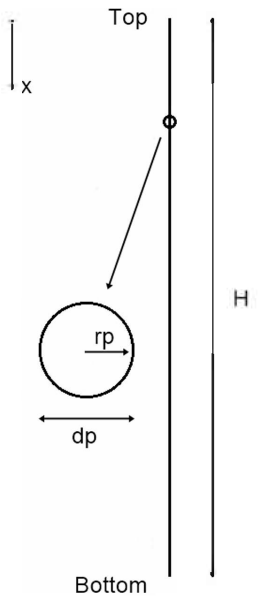

Figure 3.1: Multi geometry modelling approach - 1-D bed and 1-D particle model.

in COMSOL Multiphysics is solved with the one-dimensional, time-dependent Equation 3.1.

$$\rho_f \cdot c_{p,f} \cdot \frac{\partial T_f}{\partial t} + \rho_f \cdot c_{p,f} \cdot u_{x,f} \cdot \frac{\partial T_f}{\partial x} = \frac{\partial}{\partial x} \cdot (\lambda_f \cdot \frac{\partial T_f}{\partial x}) + Q_f \tag{3.1}$$

The derivation of the heat balance and the interpretation of the occurring terms has been described in the previous chapter. The values of the density, heat capacity and conductivity are fluid properties (depicted by the index f). The source term Q_f in the fluid domain, is the heat transferred from the particles to the fluid and will be explained in the model coupling section below. The velocity term u_x is the velocity of the fluid in the bed (cf. Fig. 3.2). The top of the bed is where the ambient air flows into the bed and at the bottom of the bed the suction is applied and the warm waste gas leaves the system. The pressure drop along the bed is not considered in the model.

The movement of the chemical species in the fluid is modelled using the following partial differential equation which accounts for the convective and diffusive transport processes in the gas.

$$\frac{\partial c_{i,f}}{\partial t} + \frac{\partial}{\partial x} \cdot (u_{x,f} \cdot c_{i,f}) = D_i \cdot \frac{\partial^2 c_{i,f}}{\partial x^2} + R_{i,f} \tag{3.2}$$

Equation 3.2 needs to be solved for every chemical species i in the model. D_i [m^2/s] is the diffusion coefficient of the chemical species i in the fluid domain. The source term $R_{i,f}$ [$mol/(m^3\,s)$] for any chemical species in the fluid domain, considers the molecules that

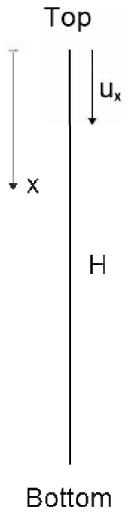

Figure 3.2: Fluid phase modelling - 1-D model of the fluid domain.

are transferred from the particle surface in the solid domain to the one-dimensional fluid domain. The flux terms for the transfer are obtained by the coupling of the two models, which is described in the model coupling section below.

3.1.2 Solid Domain Modelling

The solid phase in the sintering bed is represented by a two-dimensional spherical particle model (Fig. 3.3) whith a side length of 1 [–]. The y-dimension stands for the particle radius r_p and the x-dimension for its vertical position within the bed. The particle center is at $y = 0$ and the particle surface at $y = r_p = 1$. When implementing the differential equations of the solid domain into COMSOL the model coordinates need to be scaled with the actual particle radius and height of the bed in order to represent the real dimensions of the particles and the sintering bed. The scaling will be explained at a later point in this chapter.

The heat in the solid domain is transferred in the radial y-direction by conduction only (cf. Eq. 3.3). Radiation and convection are neglected, which leads to the energy equation without a convective term.

$$\rho_p \cdot c_{p,p} \cdot \frac{\partial T_p}{\partial t} = \frac{\partial}{\partial y} \cdot (\lambda_p \cdot \frac{\partial T_p}{\partial y}) + Q_p \tag{3.3}$$

In the time-dependent heat conduction equation the density, heat capacity and the conductivity are the properties of the solid particles (depicted by the index p), i.e the sinter mix properties. The source term Q_p is the heat from the reactions in the sinter mix, and is attained by multiplying the specific reaction enthalpies with the reaction rates.

The chemical species in the solid domain are transferred by diffusion only. Equation 3.4 is the partial differential equation that describes the species transport in the particle.

$$\frac{\partial c_{i,p}}{\partial t} = D_{e,i} \cdot \frac{\partial^2 c_{i,p}}{\partial y^2} + R_{i,p} \tag{3.4}$$

The source term $R_{i,p}$ is the production or consumption rate of the chemical species, which depends on the kinetics and stoichiometry of the reactions in the bed (cf. Chapter 2). The chemical species are transferred from the fluid domain into the particle, and are attained by the coupling of the two domains.

The solid particles are assumed to be of perfect spherical shape, which has to be considered by transferring the conservation equations into spherical coordinates. The coordinate transformation with all its implications will be described in Section 3.2.

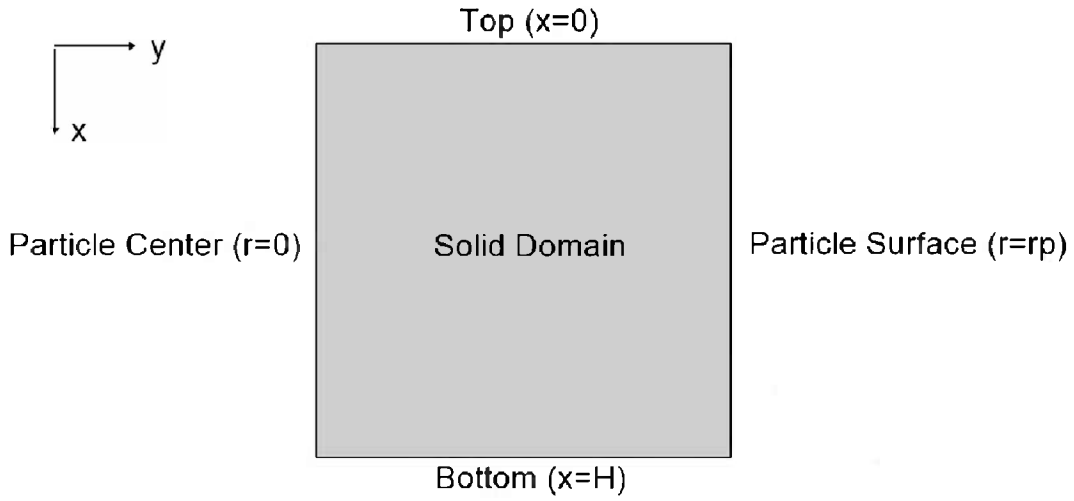

Figure 3.3: Solid phase modelling - 2-D model of the solid domain.

3.1.3 Model Coupling

As previously mentioned it is necessary that the two geometries are coupled and heat and chemical species are transferred between the two domains.

The heat from the solid domain is transferred to the fluid domain as a convective heat source by coupling the particle surface temperature T_s to the one-dimensional fluid model. The convective heat transfer is governed by Equation 3.5.

$$Q_f = A_p \cdot \alpha \cdot (T_s - T_f) \tag{3.5}$$

The source term Q_f [W/m^3], can be substituted into the heat balance in Equation 3.1. The difference between the particle surface temperature T_s and the fluid temperature T_f

is evaluated for every point along the fluid domain. The heat transfer coefficient between particle surface and fluid has to be calculated from the flow and temperature field with the help of the dimensionless Nusselt, Reynolds and Prandtl numbers (cf. Appendix). A_p is the specific particle surface. A large specific surface implies that the heat from the particle is transferred more readily which contributes to a larger value of the heat source in Equation 3.5.

The transferred heat from the fluid to the solid domain acts as a boundary flux $\dot{q}$ [W/m^2] on the surface of the particle. The convective heat flux is incorporated into the boundary condition of the solid model by the following equation.

$$\dot{q} = \alpha \cdot (T_f - T_s) \tag{3.6}$$

The considered temperatures are the fluid bulk temperature T_f obtained from the coupling with the fluid model and the surface temperature T_s evaluated for every point at the surface boundary of the solid particle model.

Chemical species such as the oxygen in the gas are transferred to the particle surface by multiplication of the concentration difference with the mass transfer coefficient β and the specific particle surface A_p (cf. Eq. 3.7). The concentration of the fluid phase $c_{i,f}$ is the bulk concentration of the chemical species i and the concentration of the solid phase $c_{i,s}$ is the species concentration at the particle surface. The calculation of the mass transfer coefficient β is explained in the Appendix.

$$\dot{n}_i = A_p \cdot \beta \cdot (c_{i,f} - c_{i,s}) \tag{3.7}$$

The species transport in the reverse direction, from the particle surface to the fluid domain, is managed by setting up flux terms for each species. The flux terms (Eq. 3.8) are treated as separate source terms and are incorporated by multiplication with the specific surface area of the particle (Eq. 3.9).

$$c_{i,flux} = D_{e,i} \cdot \frac{\partial c_{i,s}}{\partial y} \tag{3.8}$$

$$R_i = A_p \cdot c_{i,flux} \tag{3.9}$$

The species concentrations in equation 3.8 are the surface concentrations of the particles at $y = r_p$.

3.2 Spherical Particle Model

The heat transfer in the structural material of the bed has been modelled assuming a spherical particle shape. By using this assumption the solid particle can be reduced to only one dimension which decreases the calculation time due to less computational memory requirement [28]. The assumption of spherical symmetry implies that the heat transfer only depends on the radial distance r from the center of the particle. Boundary and initial conditions as well as the material properties do not vary with the space angles θ and φ.

Expanding the time dependent heat conduction equation for the solid domain (Eq. 3.3) into spherical coordinates gives Equation 3.10.

$$\rho_p \cdot c_{p,p} \cdot \frac{\partial T_p}{\partial t} = \frac{1}{r^2} \cdot \frac{\partial}{\partial r} \cdot (\lambda_p \cdot r^2 \cdot \frac{\partial T_p}{\partial r}) \tag{3.10}$$

Equation 3.10 is multiplied by r^2 to avoid division by zero at $r = 0$ resulting in the following equation

$$r^2 \cdot \rho_p \cdot c_{p,p} \cdot \frac{\partial T_p}{\partial t} = \frac{\partial}{\partial r} \cdot (\lambda_p \cdot r^2 \cdot \frac{\partial T_p}{\partial r}) \tag{3.11}$$

For modelling purposes the dimensionless radial coordinate $\hat{r}$ is introduced which consequently leads to the following definitions

$$\hat{r} = \frac{r}{r_p} \qquad \frac{\partial}{\partial r} = \frac{1}{r_p} \cdot \frac{\partial}{\partial \hat{r}}$$

The domain in the spherical particle model with $\hat{r}$ as the radial coordinate spans from 0 to 1. Substitution of the radial coordinate r in Equation 3.11 results in the final formulation of the one-dimensional time-dependent conduction equation for the spherical particle.

$$\hat{r}^2 \cdot \rho_p \cdot c_{p,p} \cdot \frac{\partial T_p}{\partial t} = \frac{\partial}{\partial \hat{r}} \cdot (\lambda_p \cdot \frac{\hat{r}^2}{r_p^2} \cdot \frac{\partial T_p}{\partial \hat{r}}) \tag{3.12}$$

The radial coordinate $\hat{r}$ corresponds to the vertical coordinate y in the solid domain model and therefore can be simply replaced. The resulting equation can be implemented into COMSOL to calculate the heat and mass transfer in the particle.

$$y^2 \cdot \rho_p \cdot c_{p,p} \cdot \frac{\partial T_p}{\partial t} = \frac{\partial}{\partial y} \cdot (\lambda_p \cdot \frac{y^2}{r_p^2} \cdot \frac{\partial T_p}{\partial y}) \tag{3.13}$$

3.3 COMSOL Implementation

The above spherical model requires some adjustment for the implementation into the software. Special care must be taken when setting up the heat flux term at the particle surface in Equation 3.6 which has not been defined in the spherical particle model yet.

3.3.1 Boundary Condition Implementation

The heat balance at the particle surface consists of the flux term from the fluid to the solid surface on the left side of the equation and the conduction in the solid particle on the right side of the equation.

$$\alpha \cdot (T_f - T_s) = \lambda_p \cdot \frac{\partial T_p}{\partial r} \tag{3.14}$$

Substitution with the dimensionless radial coordinate $\hat{r}$ changes the right hand side of the equation to

$$\alpha \cdot (T_f - T_s) = \lambda_p \cdot \frac{1}{r_p} \cdot \frac{\partial T_p}{\partial \hat{r}} \tag{3.15}$$

The boundary condition for the solid domain is defined in COMSOL as

$$g = -\vec{n} \cdot \Gamma \tag{3.16}$$

The normal vector $\vec{n}$ is defined as being of magnitude one, perpendicular to the boundary surface and oriented in the outward direction. The flux vector is obtained from the diffusive term in the conservation equation. The conservation equation for the spherical particle model has been defined in Equation 3.12.

$$\Gamma = -\lambda_p \cdot \frac{\hat{r}^2}{r_p^2} \cdot \frac{\partial T_p}{\partial \hat{r}} \tag{3.17}$$

Substituting Γ in the boundary condition (Eq. 3.16) results in

$$g = \lambda_p \cdot \frac{\hat{r}^2}{r_p^2} \cdot \frac{\partial T_p}{\partial \hat{r}} \tag{3.18}$$

Taking into account the heat balance at the particle surface (cf. Eq. 3.15), the final formulation of the boundary condition for the implementation into COMSOL can be obtained.

$$g = \frac{\hat{r}^2}{r_p} \cdot \alpha \cdot (T_f - T_s) \tag{3.19}$$

For the implementation into the solid domain model in the software $\hat{r}$ will be replaced by the radial coordinate y. The COMSOL implementation has been demonstrated for the heat transfer model, but can be applied in the same way for the purpose of modelling the mass balance.

3.4 Initial Conditions and Boundary Conditions

In order for the model to work properly and for a sound coupling between the two geometries, the initial and boundary conditions need to be defined in a way that is consistent with the previously defined modelling assumptions.

Initial conditions give information about the conditions at the starting time $t = 0$ of the simulation. In the case of heat transfer calculations, the initial conditions (IC) can be a constant temperature $T_0(t = 0)$ or a temperature distribution $T_0(x, y, z)$ at the start t_0 for the considered domain.

Boundary conditions are defined for all boundaries of the calculation domain. The boundary condition (BC) can be defined as a constant temperature or as a function of time at the boundary. Another option is to set up an incoming or outgoing heat flux at the boundary.

Not only temperatures or heat fluxes can be defined as initial or boundary conditions, but also species concentrations, pressure, velocity and other physical quantities. However, the chosen initial and boundary conditions strongly influence the results and depend on the particular case that is the scope of the study. In the following section a general view on the conditions in the sintering process will be given.

3.4.1 Initial Conditions

For the sintering model the initial temperatures and species concentrations in the solid and in the fluid domain need to be defined.

Before the ignition at the top of the sinter mix the whole sintering bed is at ambient temperature. After ignition, a significant part of the top layer is at temperatures above 1000°C which is within the range of temperature where the combustion of coke takes place. When setting up the case studies the temperatures in the solid and fluid domain can be set to any chosen values. It is also possible to virtually split one domain into many subdomains and apply different temperatures within one domain or to simulate one case study at different initial temperatures for studying the influence on the chemical reactions in the sintering bed.

The initial concentrations of carbon, oxygen, carbon monoxide, carbon dioxide, water vapour and hydrogen need to be defined to model the chemical reactions and the species transport in the sinter mix. The initial concentrations of the gaseous components can also be set to zero. The carbon concentration is only defined for the solid domain and depends on the amount of coke in the sinter mix.

3.4.2 Boundary Conditions

The boundaries of the one dimensional geometry are the in and outlet of the fluid phase. For the incoming gas any temperature that suits the scope of the study can be chosen. In COMSOL the outlet is simply defined as an *Outflow* boundary which basically means that the gas leaves the geometry at the calculated temperature.

The incoming concentrations of the gaseous components at the inlet of the fluid domain can be set to the values of ambient air which constitutes of nitrogen, oxygen and minimal amounts of carbon dioxide or to the composition of the burner gas from ignition. The inlet concentrations can be given by defining molar fractions of the species in the feed and multiplying them with the total concentration of the incoming gas. For the mass transfer calculations the outlet is also defined as an *Outflow* BC.

The solid domain boundary that represents the particle surface is coupled to the fluid domain. This means that the boundary temperatures and concentrations are defined automatically by the governing conditions within the model. Because of the assumed symmetry of the spherical particle the boundary which represents the center of the particle is defined as a zero flux boundary where the gradient is equal to zero. In the following chapter the specific case studies and set up of the COMSOL interfaces will be explained in detail.

Chapter 4

Numerical Case Studies

This chapter describes a set of case studies which have been modelled in the current master thesis. The case studies treat certain phenomena of heat and mass transfer in the sintering process. Table 4.1 summarizes the case studies that are the subject of this work. The abbreviations are introduced in order to make the referencing of the models easier, e.g. in subsequent chapters the *Heat Transfer in the Sintering Bed* model will be referred to as the *heat transfer model.*

#	**Case Study Name**	**Abbreviation**
1	Heat Transfer in the Sintering Bed	heat transfer model
2	Mass Transfer in the Sintering Bed	mass transfer model
3	Coupling of Heat and Mass Transfer in the Sintering Bed	heat and mass transfer model
4	Heterogeneous Surface Reaction	heterogeneous reaction model

Table 4.1: Comprehensive list of the simulated case studies.

A COMSOL model consists of one or more physics models. The basic set up of such a physics model involves the definition of a geometry, parameters and variables, materials and interfaces.

COMSOL provides a great number of interfaces for the simulation of multiphysics problems in the various engineering disciplines. Interfaces can be chosen from different modules, e.g. electrical engineering module, fluid dynamics module or chemical reaction engineering module, and can be combined as needed for the description of a problem. A set of differential equations to describe the underlying physical principles of the regarded phenomena is the core of each interface.

An interface is structured by nodes that define model inputs, dependent variables, initial and boundary conditions, symmetry boundaries and other options to describe the processes in the simulation. Interfaces can be coupled which adds to the complexity of the model as the simulation has to solve coupled systems of partial differential equations.

The case studies in this chapter will be explained by describing the physics models including their geometry, parameters, variables and implemented interfaces. Each interface will be treated separately and their configuration will be explained.

The case studies were set up by continually adding more complexity to the preceding case studies in order to enable a better understanding of the sintering process and multiphysics modelling in general.

4.1 Heat Transfer in the Sintering Bed Case Study

In this case study the main focus lies in modelling the heat transfer in the sintering bed. Species transport and chemical reactions are not considered in the model. The modes of heat transfer are convection and conduction in the fluid and solid domain as well as interfacial heat transfer between the two domains. To simplify calculations the sintering bed is described by a packed bed made up of monosized spherical particles. In order to account for the initial ignition of the cover layer of the sinter bed, the upper part of the bed initially is at temperatures above $1000\,K$.

The model was set up according to a multigeometry approach where the sintering bed is treated as a composite structure consisting of a fluid and a solid domain. Each of the domains has to be modelled in a separate physics model and will be coupled to one another in order to ensure interaction between the two domains. In the following paragraphs the set up and the coupling of the two domains will be described in detail.

4.1.1 Fluid Domain Model

The COMSOL interface used to model the heat transfer in the 1-D fluid domain is the *Heat Transfer in Fluids* interface. In the fluid domain model the geometry, the governing heat transfer equation and all parameters to completely describe the heat transfer in the fluid phase need to be defined by the user. The geometry of the one dimensional domain is described by simply creating an *Interval* of 0.6 m. The parameters are defined globally according to the input parameters in Table 4.2.

The values for the calculation are representative values for the sintering process taken from literature [16]. The density ρ_b and porosity ε_b are the values of the bed and are used to calculate the particle density ρ_p (cf. Eq. 2.1). For the heat capacity of the particle the value of the heat capacity $c_{p,b}$ of the bed has been used in the calculation. The values for the fluid density ρ_f, thermal conductivity λ_f and the velocity u_x are temperature dependent and therefore continuously calculated throughout the simulation process (cf. Appendix).

Parameter	Value	Unit
u_{in}	0.535	m/s
p_{atm}	0.979e5	Pa
r_p	0.003	m
A_p	807.8	m^2/m^3
$c_{p,f}$	1030.7	J/(kgK)
ρ_p	3264	kg/m^3
λ_p	5	W/(mK)
$c_{p,b}$	736.5	J/(kgK)
ρ_b	1730	kg/m^3
ε_b	0.47	–

Table 4.2: Heat transfer case study - Input parameters of the simulation.

4.1.1.1 Heat Transfer in Fluids Interface

The interface is set up by adding a time dependent study and choosing T_f as its dependent variable. The governing interface equation (Eq. 4.1) considers convective and diffusive heat transfer as well as the transferred heat Q_f from the particle surface to the fluid domain.

$$\rho_f \cdot c_{p,f} \cdot \frac{\partial T_f}{\partial t} + \rho_f \cdot c_{p,f} \cdot u_{x,f} \cdot \frac{\partial T_f}{\partial x} = \frac{\partial}{\partial x} \cdot (\lambda_f \cdot \frac{\partial T_f}{\partial x}) + Q_f \tag{4.1}$$

Heat Transfer in Fluids - The values for the density, heat capacity, thermal conductivity and the velocity are taken from Table 4.2 or alternatively, calculated by the software and implemented into the calculation.

Initial Values - At the start of the calculation the upper $0.06\,m$, which represent the high temperature zone after passing the ignition burner section in the bed, are set to $1300\,K$. The remaining area of the fluid domain is at ambient temperature of $298\,K$.

Temperature - At the inlet boundary of the one-dimensional fluid domain a constant temperature of $298\,K$ is defined.

Outflow - The outlet boundary at the bottom of the bed is defined as an *Outflow* BC.

Heat Source - In order to account for the heat that is transferred between the fluid and the solid domain the source term Q_f has to be defined.

$$Q_f = A_p \cdot \alpha \cdot (T_s - T_f) \tag{4.2}$$

The heat source described by Equation 4.2 is defined for the whole fluid domain and its magnitude depends on the particle surface temperature $T_s(x)$ and the fluid temperature $T_f(x)$. The particle surface temperature is attained from the model coupling with the solid domain. The heat transfer coefficient α is temperature dependent and is calculated during the simulation (cf. Appendix).

4.1.2 Solid Domain Model

The heat transfer in the solid domain is calculated in a separate physics model. As described in Section 3.1.2 the geometry of the solid phase is represented by a square where the x-dimension represents the distance along the bed height H and the y-coordinate a point along the particle radius r. The solid domain heat transfer is modelled using the *General Form PDE* interface.

4.1.2.1 General Form PDE Interface

The dependent variable of the interface is the particle temperature T_p. The interface provides a time dependent partial differential equation where the coefficients and terms can be defined arbitrarily to account for the heat transfer in the bed. The PDE (Eq. 4.3) is defined for the whole solid domain.

$$e_a \cdot \frac{\partial^2 T_p}{\partial t^2} + d_a \cdot \frac{\partial T_p}{\partial t} + \nabla \Gamma = f \tag{4.3}$$

The differential operator ∇ is defined for both spatial coordinates x and y which together with the time variable t are the independent variables of the interface. The mass coefficient e_a and the source term f are set to zero. The damping coefficient d_a is given in Equation 4.4. The diffusive flux Γ has to be defined for both dimensions but is set to zero for the x-direction. The flux in the y-direction is defined in Equation 4.5.

$$d_a = y^2 \cdot \rho_p \cdot c_{p,p} \tag{4.4}$$

$$\Gamma_y = -\lambda_p \cdot \frac{y^2}{r_p^2} \cdot \frac{\partial T_p}{\partial y} \tag{4.5}$$

The terms are scaled by the y-coordinate and the particle radius in order to account for the spherical shape of the particles (cf. Section 3.2 and 3.3).

General Form PDE - The values of the thermodynamic properties that are used in the calculation are listed in Table 4.2. In the damping coefficient (Eq. 4.4) the heat capacity of the bed $c_{p,b}$ is used instead of $c_{p,p}$.

Initial Values - In order to study a case that is similar to the sintering process where the top of the bed initially is at high temperatures and the propagation and distribution of heat in the bed can be examined, the solid domain is split into two parts (cf. Fig. 4.1). At the beginning (at $t = 0$) the temperature of the upper $0.06\,m$ of the geometry is set to $1300\,\mathrm{K}$, representing the heated cover layer of the sinter bed after passing the ignition burner section in the sintering process. The temperature of the remaining area is set to $298\,K$.

Flux/Source - The boundary which represents the surface of the particle is subject to a heat flux due to the temperature difference between the solid and the fluid domain. A *Flux/Source* boundary condition is set up at the surface of the particle and the flux g is defined according to Equation 4.6. The fluid bulk temperature is obtained from the coupling with the fluid domain (cf. Section 4.1.3), and the heat transfer coefficient is calculated by the software during the simulation (cf. Appendix).

$$g = \frac{y^2}{r_p} \cdot \alpha \cdot [T_{bulk} - T_p(y = r_p)] \tag{4.6}$$

Zero Flux - All remaining solid domain boundaries, i.e. the left side which represents the particle center, and the top and bottom of the square, are automatically defined as *Zero Flux* boundaries.

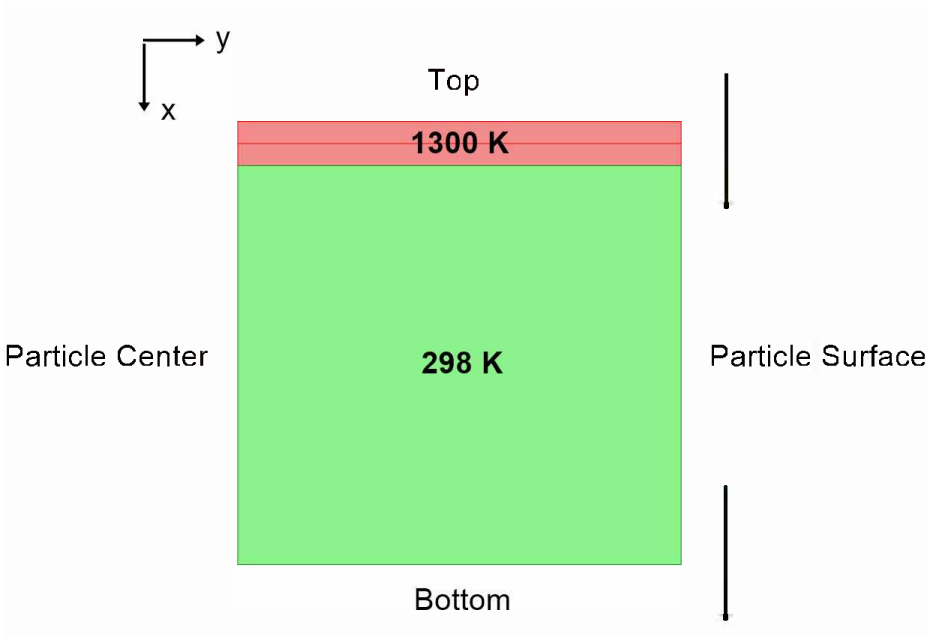

Figure 4.1: Heat transfer case study - Geometry of the fictitious 2-D solid domain.

4.1.3 Model Coupling

In the previous section the interaction of the fluid and solid domain models was demonstrated through the interfacial heat transfer from one domain to the other. The heat transfer depends on the temperature difference between the particle surface and the fluid phase. The two variables T_s and T_{bulk} are defined and made available in the fluid and solid domain respectively by using a general extrusion model coupling.

A general extrusion coupling operator is used to map an expression defined on a source domain to an expression that can be evaluated on a destination domain [29]. The one-dimensional domain is selected as the source geometric entity in order to evaluate the fluid temperature and make it available in the particle model. The destination map needs to be specified in order to map the points in the destination to the points of the source, so that the heat transfer due to the temperature difference between the corresponding points can be calculated.

In the fluid domain the extrusion is set up by coupling the x-coordinates of the fluid domain to the x-coordinates on the destination map multiplied by $0.6\,m$ (the length of the fluid domain). This is done in order to scale the height of the solid domain to the same length as the fluid domain.

The general extrusion coupling for the solid domain is similar except that for the source geometric entity only the domain boundary that represents the particle surface is selected and this time the x-coordinate in the destination map is scaled by dividing it with $0.6\,m$. Once the extrusion coupling for both domains has been set up the variable expressions for obtaining the temperatures can be defined in each physics model.

In order to make the particle temperature available in the fluid domain a variable needs to be defined in the fluid domain model. The variable is named T_s and receives the surface temperature (T_p at $y = r_p$) from the solid domain through the previously defined extrusion coupling operator (cf. Tab. 4.3). Once the variable has been defined it can be used to calculate the interfacial heat transfer in the source term of the *Heat Transfer in Fluids* interface (cf. Eq. 4.2).

Likewise the variable T_{bulk}, which obtains the temperature T_f from the fluid domain, is defined in the solid domain model (cf. Tab. 4.3). The fluid bulk temperature is implemented into Equation 4.6 to calculate the *Source/Flux* at the particle boundary. The variable names in Table 4.3 are chosen arbitrarily and are only available in the model domain where they have been defined.

Name	Variable Expression	Domain
T_s	mod2.genext2(mod2.Tp)	fluid Domain
T_{bulk}	mod1.genext1(mod1.Tf)	solid domain

Table 4.3: Heat transfer case study - General extrusion variables.

4.1.4 Meshing and Computation

The advantage of using very simple geometries for the heat transfer model is that the mesh creation is straightforward. The mesh of the one-dimensional fluid domain is created by

attributing a maximum element size of $0.0025\,m$ to the geometry. At a total length of $0.6\,m$ of the fluid domain this results in 240 elements.

The mesh of the two-dimensional solid domain geometry is illustrated in Figure 4.2. The number of elements from the left to the right side is 30 with an element ratio of 0.2 so that the element size along the y-axis decreases. The number of elements in the vertical direction is 120 and the distribution of the grid lines is uniform.

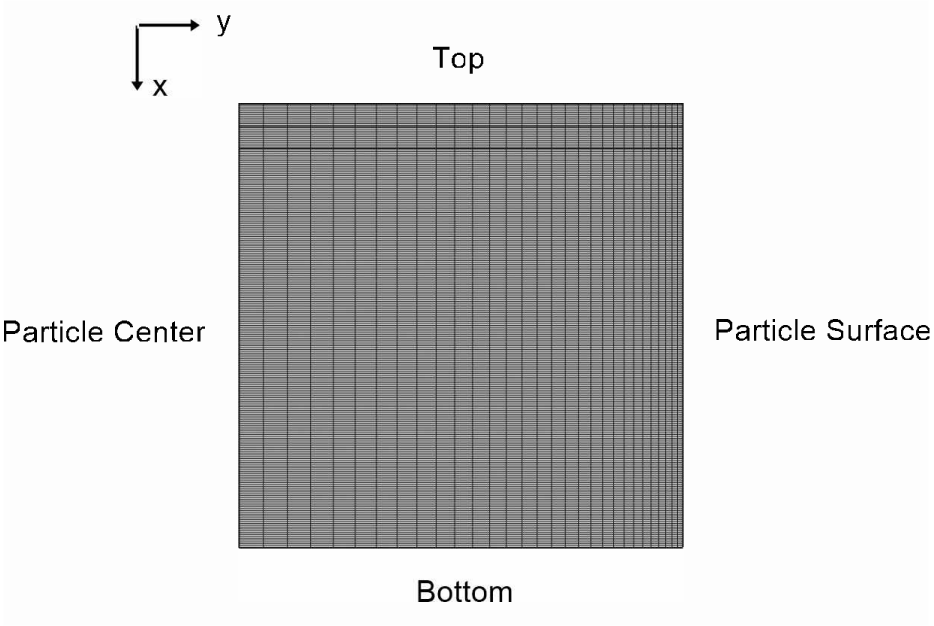

Figure 4.2: Heat transfer case study - Mesh of the 2-D solid domain.

The calculation of the heat transfer model has been carried out as a time-dependent study in order to analyse the temperature distribution in the bed at different times. The simulation stops after a calculated time of $500\,s$. Due to the simple design of the case study the calculation is quite fast and can be done with a standard computer. The results of the simulation are presented in Chapter 5.

4.2 Mass Transfer in the Sintering Bed Case Study

This case study aims to describe the transport mechanisms of the chemical species in the sintering bed. Additionally two gas phase reactions from the sintering process, i.e. the CO oxidation with oxygen and the water gas shift reaction are implemented into the model. The main scope of this case study is to model the mass transfer by diffusion into the particle, the implementation of the chemical reactions and the coupling of species concentrations between the two domains.

In the real sintering process oxygen diffuses into the particles. Inside the particles it reacts with carbon at temperatures above $1000\,K$, leading to the formation of carbon monoxide. As described by the set of reactions in Section 2.5 carbon monoxide subsequently reacts with oxygen and water vapour. As the combustion reaction has not been considered in this case study, the source of carbon monoxide and other reactants, e.g. oxygen and water vapour, is the incoming gas at the inlet of the fluid domain. The reactions are defined in the solid domain and take place as soon as the reactants are diffusing into the particle. This setup enables both diffusion modelling of chemical species into the particles and the implementation of the gas phase reactions in one case study.

As in the previous study the geometry of the model structurally resembles a packed bed reactor made up of monosized spherically shaped particles. The heat that is set free in the chemical reactions is not yet considered in this case study. The study has been carried out as a stationary study, which is contrary to the sintering process where temperature and chemical species concentrations continuously change with respect to time, and reaction rates strongly depend on the conditions in the bed. In this case study however the chemical species taking part in the reactions enter the bed with the incoming gas at the inlet of the fluid domain and the simulation will reach a steady state with constant species concentrations at the outlet of the fluid domain.

The resulting concentration profiles of the chemical species in the bed enable a better understanding of the chemical reactions in the bed. Furthermore, considering different temperatures the reaction rates, associated time scales and locations of maximum conversions in the bed can be identified.

4.2.1 Fluid Domain Model

Design and structure of the mass transfer model are very similar to the previous case study, with the only difference that the fluid domain has been shortened to $0.3\,m$. The remaining geometry, parameters and the meshing are completely identical to the heat transfer model and will not be explained again in this chapter.

4.2.1.1 Transport of Diluted Species Interface

The chemical species transport in the fluid phase has been modelled with the *Transport of Diluted Species* interface which considers convection and diffusion as the transport mechanisms. These transfer mechanisms are dependent on the fluid properties, velocity in the fluid domain and the diffusion coefficients at the considered temperature (cf. Tab. 4.4). The diffusion coefficients have been taken from a similar model that has been calculated at a system temperature of 508 K [27]. In this case study the temperature is held constant

so that all temperature dependent material properties will be calculated for that temperature and then stay constant throughout the whole simulation. The diffusion coefficients will be adapted by using Equation 4.7 which is only a rough estimate for the change with temperature, but nevertheless considered to be sufficient for the purpose of this work.

Parameter	Value	Unit
D_{CO}	$4.87 \cdot 10^{-4}$	m^2/s
D_{O_2}	$4.69 \cdot 10^{-4}$	m^2/s
D_{CO_2}	$4.69 \cdot 10^{-4}$	m^2/s
D_{H_2O}	$4.87 \cdot 10^{-4}$	m^2/s
D_{H_2}	$4.69 \cdot 10^{-4}$	m^2/s

Table 4.4: Mass transfer case study - Species diffusion coefficients in the simulation.

$$D_i(T_f) = D_i(508K) \cdot (\frac{508K}{T_f})^{\frac{3}{2}} \tag{4.7}$$

Transport of Diluted Species - The dependent variables, i.e. the concentrations of the chemical species in the fluid domain, need to be defined. The five chemical species in the homogeneous gas reactions are carbon monoxide CO, oxygen O_2, carbon dioxide CO_2, water H_2O and hydrogen H_2. For every species the partial differential equation (Eq. 4.8) needs to be solved.

$$u_{x,f} \cdot \frac{\partial}{\partial x} \cdot c_{i,f} = D_i \cdot \frac{\partial^2 c_i}{\partial x^2} + R_{i,f} \tag{4.8}$$

Initial Values - At the beginning of the calculations the initial concentrations of all chemical species are set to 10^{-6}. The fluid domain temperature is constant during the whole process. In order to investigate the influence of temperature on the chemical reaction rates, the study will be carried out at 773, 1273 and 1773 K.

Inflow - The gas containing the different chemical species enters the fluid domain on top of the one-dimensional geometry. The inlet species concentrations are the product of the total inlet concentration, which can be calculated from the ideal gas law (cf. Eq. 4.10), and the molar fraction of the chemical species at the top inlet boundary (cf. Eq. 4.9 and Tab. 4.5).

$$c_{in,i} = c_{in,tot} \cdot x_{in,i} \tag{4.9}$$

$$c_{in,tot} = \frac{p_{atm}}{R \cdot T_{in}} \tag{4.10}$$

Chemical Species	Molar Fraction
$x_{in,CO}$	0.0291
x_{in,O_2}	0.1453
x_{in,CO_2}	0
x_{in,H_2O}	0.0582
x_{in,H_2}	0
$x_{in,inert}$	0.7674

Table 4.5: Mass transfer case study - Molar fraction of the chemical species in the gas feed [16].

Outflow - The outlet boundary is defined as an *Outflow* BC meaning that the chemical species in the gas leave the fluid domain at the calculated concentrations.

Reactions - A *Reaction* node that implements the species flux from the particle surface into the fluid domain is added to the interface. The reaction terms for each species are calculated by multiplying the specific surface area of the particle with the species flux from the fluid domain obtained from the general extrusion operator (cf. Eq. 4.11).

$$R_i = -A_p \cdot c_{i,flux} \tag{4.11}$$

4.2.2 Solid Domain Model

As in the heat transfer case study the solid domain is modelled with the *General Form PDE* interface.

4.2.2.1 General Form PDE Interface

The interface equation has already been presented in the previous case study (cf. Eq. 4.3). The mass coefficient e_a and source term f of the PDE are set to zero. The damping coefficient d_a and flux term Γ in the y-direction are defined in Equations 4.12 and 4.13.

$$d_a = y^2 \tag{4.12}$$

$$\Gamma_y = -D_{e,i} \cdot \frac{y^2}{r_p^2} \cdot \frac{\partial c_{i,p}}{\partial y} \tag{4.13}$$

Implementing the two terms into the partial differential equation of the interface leads to Equation 4.14.

$$y^2 \cdot \frac{\partial c_{i,p}}{\partial t} = \frac{\partial}{\partial y} \cdot (D_{e,i} \cdot \frac{y^2}{r_p^2} \cdot \frac{\partial c_{i,p}}{\partial y}) \tag{4.14}$$

General Form PDE - In this node the damping coefficient and flux term for each chemical species are put into the interface. The equation needs to be solved for every dependent variable $c_{i,p}$ of the solid domain.

The chemical species in the solid particles are transported by molecular diffusion along the radial y-coordinate only. $D_{e,i}$ is the effective diffusion coefficient, obtained by multiplying the diffusion coefficient D_i with the particle porosity ε_p. It is used to calculate the diffusion inside the pores of the solid matrix of the particles, which is slower than in the bulk phase. Due to the lack of porosity values for the particles the effective diffusion coefficient in this case study is obtained by multiplying the diffusion coefficient with the porosity ε_b of the bed. The difference between these two porosity values is that ε_b describes the void fraction between the particles in the bed whereas ε_p describes the microstructure of a particle which is of interest when dealing with mass transfer into the particle.

Initial Values - At the beginning of the calculation all initial concentrations of the chemical species in the solid domain are set to 10^{-6}. The initial temperature in the solid domain will change depending on the simulated case.

Dirichlet Boundary Conditions - The particle surface concentration is attained by implementing a *Dirichlet Boundary Condition* (at $y = r_p$) which prescribes the concentration value ($c_{i,bulk}$) from the coupling with the fluid domain to the solid domain boundary.

Zero Flux - If not defined otherwise the remaining boundaries, i.e. the particle center (at $y = 0$), the top and bottom of the solid domain are defined as zero flux boundaries.

Source - The chemical reaction rates R_{react2} and R_{react3} and their reaction constants are defined as global variables outside of both physics models (cf. Tab. 4.6). Their values which are dependent on the temperature and species concentrations in the solid domain, will be calculated during the simulation and implemented into the source terms of the *General Form PDE* interface (cf. Tab. 4.7). Depending on the direction and stoichiometry of the chemical reaction the concentration of the species in the solid domain will either increase or decrease.

4.2.3 Model Coupling

The fluid and solid domain in the mass transfer case study are coupled by setting up a general extrusion operator. The flux $c_{i,flux}\,[mol/(m^2 s)]$ from the particle surface to the

Global Variable	Variable Expression
R_{react2}	$k_2 \cdot (c_{CO,p} \cdot c_{O_2,p}^{\frac{1}{2}} \cdot c_{H_2O,p}^{\frac{1}{2}})$
k_2	$1.8 \cdot 10^8 \cdot \exp(\frac{E_a}{R \cdot T})$
R_{react3}	$k_3 \cdot (c_{CO,p} \cdot c_{H_2O,p} - \frac{c_{CO_2,p} \cdot c_{H_2,p}}{K_{eq}})$
k_3	$2.78 \cdot 10^3 \cdot \exp(-\frac{1510}{T})$
K_{eq}	$0.0265 \cdot \exp(\frac{3968}{T})$

Table 4.6: Mass transfer case study - Global variables of the simultation.

Chemical Species	Source Term Expression
$\dot{S}_{CO}$	$y^2 \cdot (-R_{react2} - R_{react3})$
$\dot{S}_{O_2}$	$y^2 \cdot (-\frac{1}{2} \cdot R_{react2})$
$\dot{S}_{CO_2}$	$y^2 \cdot (R_{react2} + R_{react3})$
$\dot{S}_{H_2O}$	$y^2 \cdot (-R_{react3})$
$\dot{S}_{H_2}$	$y^2 \cdot (R_{react3})$

Table 4.7: Mass transfer case study - Source terms of the chemical reaction.

fluid domain is calculated by Equation. 4.15.

$$c_{i,flux} = D_i \cdot \frac{y}{r_p} \cdot \frac{\partial c_{i,p}(y = r_p)}{\partial y} \tag{4.15}$$

In the solid domain model the chemical species concentration from the fluid phase is attained through the general extrusion operator and directly applied to the surface boundary of the particle (cf. Tab. 4.8). The y at the end of the particle concentration expression (ci_p) in Table 4.8 is the COMSOL notation for calculating the first derivative with respect to y.

Name	Variable Expression	Domain
$c_{i,flux}$	mod2.genext2(Di*mod2.ci_py*y/r_p)	fluid Domain
$c_{i,bulk}$	mod1.genext1(mod1.ci_f)	solid domain

Table 4.8: Mass transfer case study - General extrusion variables (COMSOL notation).

4.2.4 Meshing and Computation

Since the geometry of the mass transfer case study is identical to that of the heat transfer case study the meshing will not be explained again here. After the meshes of both geometries have been set up the case study is ready for calculation.

The study has been carried out as a stationary study. Once the process reaches a steady state, the solution provides a characteristic concentration profile of the chemical species in the bed. The results of the simulations are presented in Chapter 5 of this work.

4.3 Coupling of Heat and Mass Transfer in the Sintering Bed Case Study

The two previous case studies treated the set up of a model of the heat transfer and a model to study mass transfer in the sintering bed. In order to study the interaction between the heat and mass transfer the third case study combines the two previous studies into one model. Mass transfer, and more specifically chemical reactions in the bed are influenced by heat transfer and at the same time are a major contributor to temperature changes due to the heat of the reactions that is either consumed or set free during the reactions. In iron ore sintering the heat from the reactions is responsible for the high temperatures and the characteristic temperature profile in the bed. This model focuses on the temperature change due to the homogeneous reactions that have already been modelled in the mass transfer model (cf. Section 4.2).

The challenge of this case study is merging the two models into one single case study. The general structure of the previous case studies will be left unaltered, with the only difference that in this study both physics models consist of two interfaces. The two interfaces describing the heat and mass transfer in the fluid domain are the *Heat Transfer in Fluids* and the *Transport of Diluted Species* interfaces. For the modelling of the solid domain two *General Form PDE* interfaces will be implemented into the model. In this case study not only the two domains are interacting, also the interfaces in one domain are influencing each other. The set up of the fluid and solid models, the model coupling and the meshing and computation of the case study will be described in the subsequent sections.

4.3.1 Fluid Domain Model

As mentioned above the set up of the fluid domain model is similar to the fluid domain in the previous case studies. The fluid domain is represented by a one-dimensional *Interval* of $0.3\,m$ where the heat is transferred by conduction and convection and mass transfer is achieved by molecular diffusion and the movement of the fluid. The heat transfer is calculated by the *Heat Transfer in Fluids* interface and the mass transfer by the *Transport of Diluted Species* interface. Both interfaces are added to the fluid domain and defined according to the following configurations.

4.3.1.1 Heat Transfer in Fluids Interface

Heat Transfer in Fluids The fluid phase temperature T_f is defined as the dependent variable of the interface. The governing equation and input parameters for the thermal conductivity, density and heat capacity are the same as in the heat transfer case study (cf. Eq. 4.1 and Tab. 4.2).

Initial Values - To study the influence of the temperature on heat and mass transfer the study will be carried out at initial fluid temperatures of either 773, 1273 or $1773\,K$.

Temperature - Setting up a *Temperature* boundary condition at the inlet of the fluid domain prescribes a fixed temperature to the entering gas. In accordance with the initial condition the boundary temperature will be set to 773, 1273 or $1773\,K$.

Outflow - The outlet of the fluid domain is defined as an *Outflow* boundary condition.

Heat Source - To account for the heat that is transferred from the surface of the solid particle to the fluid domain a *Heat Source* node is added to the *Heat Transfer in Fluids* interface. The heat is transferred through interfacial convection and is dependent on the specific particle surface area A_p, the heat transfer coefficient α and the temperature difference between the fluid and the particle surface (cf. Eq. 4.16). The surface temperature T_s is obtained through coupling with the solid domain.

$$Q_f = A_p \cdot \alpha \cdot (T_s - T_f) \tag{4.16}$$

4.3.1.2 Transport of Diluted Species Interface

The *Transport of Diluted Species* interface is also added to the fluid domain model which means that it is defined for the same geometry, coordinate system and unit system as the *Heat Transfer in Fluids* interface. As in the mass transfer case study the dependent variables are the species concentrations $c_{i,f}$ in the fluid domain.

Transport of Diluted Species - The interface is subject to the same equation as in the mass transfer case study (cf. Eq. 4.8) and also uses the same velocity and diffusion coefficients of the chemcical species.

Initial Values - At the beginning of the calculation the initial concentrations in the solid domain are set to 10^{-6}.

Inflow - The boundary condition ascribes the concentrations of the incoming chemical species to the inlet at the top of the fluid domain. The concentration values are calculated from the molar fraction in the incoming gas and the total gas concentration

at the inlet calculated by the ideal gas law (cf. Eq. 4.9). The values are the same as in the mass transfer model and can be found in Table 4.5.

Outflow - The outlet of the fluid domain is defined as an *Outflow* boundary condition which means that the chemical species in the fluid leave the domain at the calculated concentrations.

Reactions - A *Reactions* node is added to the interface with defined expressions for each chemical species. The reaction terms are defined as the product of the specific surface area of the particle and the species flux obtained from the coupling with the solid domain (cf. Eq. 4.17).

$$R_i = -A_p \cdot c_{i,flux} \tag{4.17}$$

4.3.2 Solid Domain Modelling

The heat and the mass transfer in the solid domain are both defined in a *General Form PDE* interface.

4.3.2.1 General Form PDE Interface (Heat Transfer)

The interface equation in the general form has already been described in the previous case study 1. The dependent variable of the interface is the solid domain temperature T_p.

General Form PDE 1 - To define the heat transfer in the solid domain the flux term Γ and damping coefficient d_a need to be defined in the *General Form PDE* node of the interface. The mass term e_a and the source term f are set to zero. The damping coefficient is a scalar and is defined according to Equation 4.18. The flux term is a vector and is defined only in the y-direction along the radius of the particle (cf. Eq. 4.19).

$$d_a = y^2 \cdot \rho_p \cdot c_{p,p} \tag{4.18}$$

$$\Gamma_y = -\lambda_p \cdot \frac{y^2}{r_p^2} \cdot \frac{\partial T_p}{\partial y} \tag{4.19}$$

Initial Values - As in the fluid domain the temperature at the start of the calculation is set to 773, 1273 or 1773 K.

Flux/Source - A boundary flux g is prescribed to the solid domain boundary (at $y = r_p$) representing the particle surface. The flux depends on the heat transfer coefficient α and the temperature difference between the fluid domain T_{bulk} and the particle

surface $T_p(y = r_p)$ (cf. Eq. 4.20). The bulk temperature of the fluid is obtained through coupling of the domains (cf. model coupling section below).

$$g = \frac{y^2}{r_p} \cdot \alpha \cdot (T_{bulk} - T_p(y = r_p)) \tag{4.20}$$

Source - Heat that is either consumed or produced in the chemical reactions contributes to the heat balance of the solid domain and has to be accounted for by adding a *Source* node to the PDE interface. The node is defined for the whole solid domain and described by the source term f in Equation 4.21. The heat source term is the sum of the heat from both homogeneous reactions (R 2.13 and R 2.14) which are calculated by multiplying the reaction rate expressions R_{react} with the heat H_r of the considered reactions.

$$f = -y^2 \cdot (R_{react2} \cdot H_{r,2} + R_{react3} \cdot H_{r,3}) \tag{4.21}$$

4.3.2.2 General Form PDE Interface (Mass Transfer)

The mass transfer and chemical reactions in the solid domain are also modelled with a *General Form PDE* interface. The interface is added to the same physics model as the PDE interface for the heat transfer which means that it is subject to the same geometry, coordinate system, unit system and mesh. Subsequently the interface and all its defined nodes will be explained. The dependent variables of the interface are the solid phase concentrations of the chemical species that take part in the homogeneous reactions of the sintering process.

General Form PDE - The general interface equation has already been described in Equation 4.3. The mass coefficient e_a and source term f are set to zero. The vector of the conservative flux term is defined only in the y-coordinate according to Equation 4.22. The damping coefficient d_a is y^2. Both terms are implemented into the differential equation of the interface.

$$\Gamma_y = -D_{e,i} \cdot \frac{y^2}{r_p^2} \cdot \frac{\partial c_{i,p}}{\partial y} \tag{4.22}$$

Initial Values - All chemical species concentration values are set to 10^{-6} at the beginning of the simulation.

Dirichlet Boundary Conditions - The concentration at the boundary of the solid domain that represents the surface of the particle (at $y = r_p$) is equal to the concentration of the fluid domain $c_{i,bulk}$. The bulk concentration of the fluid domain is attained by coupling of the domains with the general extrusion operator (cf. Chapter 4.1.3).

Source - The chemical species concentrations in the solid domain are subject to the reaction rates. To account for the change in concentration due to the chemical reactions a *Source* node is added to the PDE interface and the species balance for each chemical species is entered as a source term (cf. Tab. 4.7).

4.3.3 Model Coupling

The two physics models in the case study are coupled with each other so that the surface temperature and concentrations from the solid domain are made available in the fluid domain and that fluid temperature and concentrations from the fluid domain are available for calculations in the solid model. This has been achieved through the set up of the *General Extrusion* operator which maps the fluid domain to the particle surface and vice versa. The temperature and concentrations are obtained by defining variables in the domain models.

The variables of the fluid domain are identical to those of previous two models and are summarized in Table 4.9. The flux variables are the first derivative of the concentration values $c_{i,p}$ of the solid domain species with respect to y multiplied by the diffusion coefficient and the quotient of y and r_p.

Name	Variable Expression
T_s	mod2.genext2(mod2.Tp)
$c_{CO,flux}$	mod2.genext2(D_CO*mod2.cCO_py*y/rp)
$c_{O_2,flux}$	mod2.genext2(D_O2*mod2.cO2_py*y/rp)
$c_{CO_2,flux}$	mod2.genext2(D_CO2*mod2.cCO2_py*y/rp)
$c_{H_2O,flux}$	mod2.genext2(D_H2O*mod2.cH2O_py*y/rp)
$c_{H_2,flux}$	mod2.genext2(D_H2*mod2.cH2_py*y/rp)

Table 4.9: Heat and mass transfer case study - Fluid domain coupling (COMSOL notation).

The variables of the solid model are defined as in Table 4.10. The variable expressions refer to the general extrusion operator (*genext*1) in the physics model (*mod*1) of the fluid domain.

Apart from the coupling of the two domains also the interfaces in the solid domain are coupled. In the solid domain model the mass transfer PDE interface interacts with the heat transfer PDE interface through the heat that is released as a consequence of the chemical reactions in the bed. It has been accounted for by adding a heat source term into the *General Form PDE* of heat transfer, which is the reaction rate multiplied by the specific enthalpy of the reaction.

Name	Variable Expression
T_{bulk}	mod1.genext1(mod1.Tf)
$c_{CO,bulk}$	mod1.genext1(mod1.cCO_f)
$c_{O_2,bulk}$	mod1.genext1(mod1.cO2_f)
$c_{CO_2,bulk}$	mod1.genext1(mod1.cCO2_f)
$c_{H_2O,bulk}$	mod1.genext1(mod1.cH2O_f)
$c_{H_2,bulk}$	mod1.genext1(mod1.cH2_f)

Table 4.10: Heat and mass transfer case study - Solid domain coupling (COMSOL notation).

The temperature distribution in the solid domain model on the other hand influences the chemical reactions by its influence on the reaction rate expressions. The reaction rates and its frequency factors are defined as variables at a global level outside of the physics models. Table 4.11 shows how the temperature and the concentrations from the solid domain are implemented into the reaction rate expressions.

Global Variable	Variable Expression
R_{react2}	k1*mod2.cCO_p*mod2.cO2_p^0.5*mod2.cH2O_p^0.5
k_2	1.8e8*exp(Ea/Rc/mod2.Tp)
R_{react3}	k2*(mod2.cCO_p*mod2.cH2O_p-mod2.cCO2_p*cH2_p/Keq)
k_3	2.78e3*exp(-1510/mod2.Tp)
K_{eq}	0.0265*exp(3968/mod2.Tp)

Table 4.11: Heat and mass transfer case study - Reaction rate expressions (COMSOL notation).

As the reaction rates are again dependent on the temperature it is quite obvious that the interaction of heat and mass transfer makes the calculation and estimation of the simulation results a lot more difficult.

4.3.4 Meshing and Computation

The meshing of the two geometries is identical to the two previous case studies and has already been explained in Section 4.1.4. Three different simulations have been carried out as stationary studies with incoming gas temperatures of 773, 1273 and 1773 K. The results of the simulations are presented Chapter 5.

4.4 Heterogeneous Surface Reaction Case Study

The fourth case study aims at simulating heterogeneous reactions with COMSOL Multiphysics in order to describe the combustion reaction of carbon in the sintering process (cf. Eq. 2.11, 2.12 and 2.15). The approach used to simulate the heterogeneous combustion reaction was to model it as a surface reaction in a flow cell. An already existing COMSOL Multiphysics tutorial case study that models surface reactions in a biosensor was used as a reference [30]. The case study combines surface reactions and mass transport in a laminar fluid stream. The gas carries oxygen into the cell which reacts with carbon on the surface of the spheres in order to build carbon monoxide which is released back to the gas stream. Additionally a heat transfer interface that accounts for the heat of the surface reactions was implemented into the case study.

4.4.1 Model Definition

The case study is set up in a three-dimensional flow cell that contains an array of spheres. The surface reactions take place on the surface of the spheres and are modelled with the *Surface Reactions* interface. As in the previous case studies the mass transfer in the fluid has been modelled with the *Transport of Diluted Species* interface, but unlike before where the fluid motion was subject to a constant velocity the motion of the fluid in the flow cell has been modelled with the *Laminar Flow* interface. The *Heat Transfer in Fluids* interface was used to calculate the change in temperature. In the subsequent sections the geometry, the defined parameters and variables and the set up of the interfaces will be described.

4.4.1.1 Geometry

Before the actual modelling can be done the geometry of the case study has to be built. While the geometry of the previous case studies was quite simple and straightforward this case study is subject to a more complex three-dimensional geometry. By replacing the pillars in the geometry of the COMSOL tutorial with spheres the geometry has been set up in a separate file, then imported into the case study [30]. The cell is quite small with a length of $12 \cdot 10^{-3}\,m$, a width of $6.9 \cdot 10^{-3}\,m$ and a height of $10^{-3}\,m$.

The geometry of the case study holds seven rows of spheres with four spheres in each row (cf. Fig. 4.3). Adjoining rows are slightly offset so that the neighbouring spheres of different rows are not directly next to each other.

Due to two planes of symmetry in the flow cell this setup allows a reduction of the geometry (cf. Fig. 4.4). Now the modelling domain is made up of only one fourth of the full geometry which will significantly shorten the calculation time of the case study.

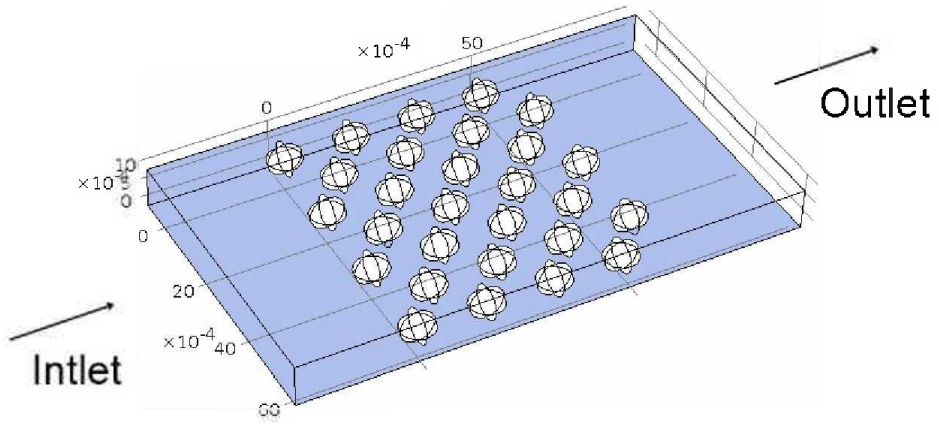

Figure 4.3: Heterogeneous reaction case study - 3-D geometry of the flow cell. Cell size: $(12 \cdot 10^{-3}\, m)$ x $(6.9 \cdot 10^{-3}\, m)$ x $(1 \cdot 10^{-3}\, m)$; Sphere diameter: $8 \cdot 10^{-4}\, m$; Distance between two spheres in a row: $8 \cdot 10^{-4}\, m$;

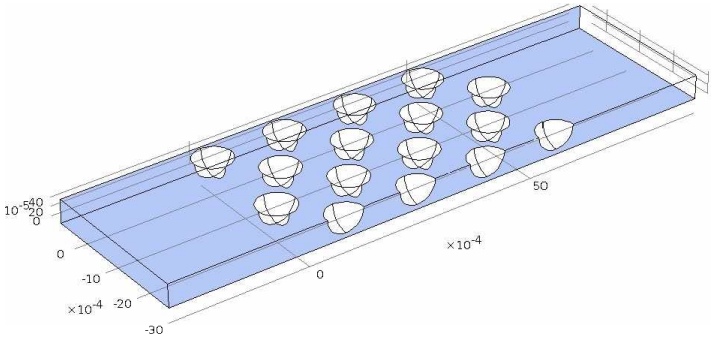

Figure 4.4: Heterogeneous reaction case study - 3-D geometry of the modelling domain.

4.4.1.2 Parameters and Variables

Parameters like the diffusion coefficients and the composition of the fluid phase are the same as in previous studies. The inlet velocity u_{in} has been scaled down in relation to the length of the cell so that their ratio is about the same as the velocity to length ratio of the fluid domain from the previous case studies. Material properties like the density, heat capacity, specific heat and the viscosity of the gas have been taken from COMSOLs material library. To carry out the calculations of the case study air has been selected to represent the properties of the gas. The inlet temperature, total inlet concentration and the reaction enthalpy of coke combustion along with the already mentioned parameters are defined in Table 4.12.

Parameter	Value	Unit
u_{in}	0.08	m/s
D_{CO}	$4.87 \cdot 10^{-4}$	m^2/s
D_{O_2}	$4.69 \cdot 10^{-4}$	m^2/s
$x_{O_2,in}$	0.1453	–
T_{in}	1300	K
p_{atm}	$0.979 \cdot 10^5$	Pa
$c_{tot,in}$	$\frac{p_{atm}}{R \cdot T_{in}}$	mol/m^3
H_{react}	–110	kJ/mol

Table 4.12: Heterogeneous reaction case study - Input parameters of the simulation.

The reaction rate R_{react} [31], rate constant k, frequency factor A, activation energy Ea and the temperature dependent diffusion coefficients D_i are defined as variables according to Table 4.13.

4.4.1.3 Laminar Flow Interface

Assuming a laminar flow regime the fluid flow in the cell was modelled with the *Laminar Flow* interface.

Laminar Flow - The flow is given by the Navier Stokes equations (cf. Eq. 4.23), defined for a stationary and incompressible flow.

$$\rho_f \cdot \mathbf{u} \cdot \nabla \mathbf{u} = \nabla[-p \cdot \mathbf{I} + \eta_f \cdot (\nabla \mathbf{u} + (\nabla \mathbf{u})^T) - \frac{2}{3} \cdot \eta_f (\nabla \cdot \mathbf{u}) \cdot \mathbf{I}] \tag{4.23}$$
$$\nabla \cdot (\rho_f \cdot \mathbf{u}) = 0$$

Parameter	Value	Unit
$R_{s,react}$	$k \cdot c_{O_2} \cdot cshr.theta\_free$	$\mathrm{mol/(m^2\,s)}$
k	$A \cdot mod1.T \cdot \exp(-\frac{Ea}{R \cdot mod1.T})$	m/s
A	1.692	$\mathrm{m/(s\,K)}$
Ea	$0.0582 \cdot 10^5$	J/mol
D_{CO}	$4.87 \cdot 10^{-4} \cdot (\frac{508K}{mod1.T})^{\frac{3}{2}}$	$\mathrm{m^2/s}$
D_{O_2}	$4.69 \cdot 10^{-4} \cdot (\frac{508K}{mod1.T})^{\frac{3}{2}}$	$\mathrm{m^2/s}$

Table 4.13: Heterogeneous reaction case study - Input variables of the simulation (COMSOL notation).

The density $\rho_f\,[kg/m^3]$, the viscosity $\eta_f\,[kg/(m \cdot s)]$ are fluid properties and are obtained from the material library. The dependent variables $\mathbf{u}\,[m/s]$ and $p\,[Pa]$ are the velocity vector and pressure in the flow cell.

Fluid Properties - Density and viscosity values of the fluid are obtained from the material library. Only the temperature and atmospheric pressure have to be put into the model in order to describe the flow behaviour. As in the heat transfer case study the temperature of the fluid has been set to $1300\,K$.

Wall - To all boundaries that are neither inlets, outlets or symmetry planes of the cell, i.e. the side walls of the cell and surfaces of the sphere a no slip boundary condition was assigned. This is done automatically by the software for all undefined boundaries.

Initial Values - At the beginning the initial values for the velocity and pressure are set to zero.

Inlet - A normal inflow velocity $u_{in}\,[m/s]$ of $0.08\,[m/s]$ is assigned to the inlet boundary.

Outlet - At the outlet the viscous stresses are ignored and by setting the pressure value to zero the absolute pressure at the outlet is equal to the previously defined atmospheric pressure p_{atm}.

Symmetry In the *Symmetry* node a symmetry boundary condition is assigned to the two symmetry planes of the reduced geometry.

The calculated flow field from the *Laminar Flow* interface will serve as an input in the *Transport of Diluted Species* interface and the *Heat Transfer in Fluids* interface.

4.4.1.4 Transport of Diluted Species Interface

The mass transport of chemical species in the fluid has been modelled with the *Transport of Diluted Species* interface. The dependent variables of the interface are the concentrations of oxygen c_{O_2} and carbon monoxide c_{CO} in the gas stream. The configuration of the interface and its nodes will be explained in the subsequent paragraphs.

Transport of Diluted Species - In the previous case studies the concept and underlying equations of the *Transport of Diluted Species* interface have already been described in detail (cf. Section 4.2.1). The time-dependent differential equation that describes the mass transfer in the interface is given in Equation 4.24.

$$\frac{\partial c_i}{\partial t} + \nabla \cdot (-D_i \nabla c_i) + \mathbf{u} \cdot \nabla c_i = 0 \tag{4.24}$$

Convection and Diffusion - In order to describe the motion of the fluid in the flow cell, the velocity field that has been calculated in the *Laminar Flow* interface is used as the model input for $\mathbf{u}$. Apart from the velocity vectors the diffusion coefficients are defined as isotropic with the values defined previously in the parameter section.

Initial Values - The oxygen and carbon monoxide concentrations in the flow cell at the beginning of the calculation are zero.

Inflow - Another analogy to the previous case studies is the definition of the concentrations in the incoming gas stream. For the sake of simulating the combustion of coke in the bed only the oxygen concentration in the incoming gas is of importance. It is calculated by multiplying the total concentration of the feed with the molar fraction of oxygen in the feed (cf. Eq. 4.25). For the calculation of the inlet oxygen concentration the same molar fraction ($x_{in,O_2} = 0.1453$) as in the other case studies has been used. Equation 4.26 together with the temperature and pressure values from the *Laminar Flow* interface has been used to calculate the total feed concentration.

$$c_{in,O_2} = c_{in,tot} \cdot x_{in,O_2} \tag{4.25}$$

$$c_{in,tot} = \frac{p_{atm}}{R \cdot T_{in}} \tag{4.26}$$

Outflow - An *Outflow* boundary condition (cf. Eq. 4.27) has been prescribed to the boundary that represents the outlet of the modelling domain.

$$\mathbf{n} \cdot (-D \nabla c) = 0 \tag{4.27}$$

Symmetry - Just as in the *Laminar Flow* interface a symmetry boundary condition has been added to the two symmetry planes.

Flux - In order to describe the in and outgoing species fluxes at the surfaces of the spheres, a flux boundary condition that is dependent on the local concentrations of oxygen has been applied to all the reacting surfaces. The net molar flux at the surface that is in accordance with the stoichiometry of the reaction is given in Equation 4.28.

$$N = -R_{s,react} + 2 \cdot R_{s,react} \tag{4.28}$$

The net flux in Equation 4.28 describes that according to the stoichiometry of the combustion reaction for each reacting mole of O_2 at the surface, two moles of CO are created. The term $R_{s,react}\,[mol/(m^2 \cdot s)]$ is the surface reaction rate of the heterogeneous reaction. In the *Flux* node an inward flux - a flux from the reacting surface into the domain - has to be defined for each species in the fluid phase. The defined oxygen and carbon monoxide fluxes are given by

$$N_{O_2} = -R_{s,react} \tag{4.29}$$

$$N_{CO} = 2 \cdot R_{s,react} \tag{4.30}$$

The surface flux in the *Transport of Diluted Species* interface is coupled to the *Surface Reactions* interface, which will be described in the following paragraphs.

4.4.1.5 Surface Reactions Interface

With the *Surface Reactions* interface it is possible to model reactions and transport of surface species on a boundary, i.e. the modelling of the combustion reaction on the particle surface and the transport in the tangential direction of the surface governed by Fick's law. The dependent variables of the interface are the species surface concentrations $c_{s,i}$.

Surface Reactions - The Modelling domain of the *Surface Reactions* interface is the surface of the spheres in the flow cell. The dependent variable in this model is the concentration of the adsorbed oxygen c_{s,O_2}. The governing equation of the interface is given by Equation 4.31, where $R_{s,i}$ $[mol/(m^2 \cdot s)]$ denotes the sum of all sources due to the surface reactions.

$$\frac{\partial c_i}{\partial t} + \nabla_t \cdot (-D_{s,i} \nabla_t c_{s,i}) = R_{s,i} \tag{4.31}$$

Surface Properties - In this node, the sites of the reacting surfaces are defined by assigning a site density value Γ_s which in this case study represents the surface concentration of carbon. The site density value is set to $4 \cdot 10^{-5}\,[mol/m^2]$. In accordance to the stoichiometry the site occupancy number $\sigma_{c_{s,O_2}}$ [-] is set to 2 which indicates that 2 moles of O_2 react with one mole of C. Setting the diffusion coefficient $D_{s,i}$ to zero, implies that surface diffusion is not considered in the case study.

Initial Values - The surface concentration of oxygen c_{s,O_2} is zero at the beginning of the simulation.

Reactions - This node couples the reaction rate of the surface species to the *Transport of Diluted Species* interface. The balance for the surface species c_{s,O_2} is equal to 0.5 times $R_{s,react}\,[mol/(m^2 \cdot s)]$ which is the previously defined reaction rate of the surface species (cf. Tab. 4.13).

4.4.1.6 Heat Transfer in Fluids Interface

The *Heat Transfer in Fluids* interface has been added to the fluid domain to calculate the temperature distribution in the flow cell. The dependent variable is the fluid temperature T_f.

Heat Transfer in Fluids - In order to calculate the heat transfer the calculated velocity field from the *Laminar Flow* interface is implemented into the interface. The density, heat capacity and thermal conductivity are taken from the material library and the pressure has already been defined in the parameter section above.

Initial Values - The initial temperature in the fluid phase is set to $1300\,K$.

Temperature - A fixed temperature of $1300\,K$ is defined at the gas inlet.

Outflow - The gas outlet is defined as an *Outflow* BC.

Symmetry - As in the previous interfaces the symmetry planes of the geometry need to be defined accordingly.

Heat Flux - The heat of the reaction is accounted for by adding a *Heat Flux* node to the interface. The heat flux is applied to the spherical surfaces where the reactions take place. It is dependent on the surface reaction rate and the heat of combustion (cf. Eq. 4.32).

$$\dot{q} = -H_{react} \cdot R_{react} \tag{4.32}$$

This case study is a good example for the coupling of fluid flow, mass transport in a fluid and on a surface and heat transfer, a problem that is quite common in chemical engineering. In the subsequent paragraphs the meshing and computation of the case study will be described.

4.4.2 Meshing and Computation

An unstructured triangular mesh is created on the reacting surface of the spheres. This is done by choosing *Free Triangular* from the mesh menu and applying a maximum element size of $5 \cdot 10^{-5}\,m$. To the remaining modelling domain a tetrahedral mesh is applied by choosing *Free Tetrahedral* from the menu and a maximum element size of $2{\cdot}10^{-4}\,m$. Selecting the *Build All* button starts the meshing process which depending on the computational power can take some time to complete the mesh. The triangular mesh on the reacting surfaces consists of 2,157 elements. The tetrahedral mesh of the remaining fluid domain is made up of 128,848 elements.

A one way coupling between the stationary flow field and the mass transport means that the equations for the laminar flow need only be solved once. This is achieved by setting up a stationary study for the *Laminar Flow* interface, of which the results will then be implemented into the time-dependent heat and mass transfer study. The second step during the calculation solves for the *Transport of Diluted Species* interface, the *Surface Reaction* interface and the *Heat transfer in Fluids* interface during a simulation time interval of $0.1\,s$.

The concentration of the surface species will be of many orders of magnitude lower compared to the concentration in the fluid phase. To help convergence manual scales for the concentration variables will be provided. The scale set for the concentration of the surface species is 10^{-7} while it is set to 10 for the species in the fluid. After the solver configuration is completed the case study is ready for computation. The resulting data will be presented in the following chapter.

Chapter 5

Results and Discussion

The numerical results from the case studies and the discussion of certain aspects and implications for further studies will be the subject of this chapter. The case studies will be treated separately and in the same order as for their description in the previous chapter.

5.1 Results of the Heat Transfer in the Sintering Bed Case Study

The results of the *Heat Transfer in the Sintering Bed* model are presented as temperature profiles of the solid and fluid domain at different times of the simulation. The results are strongly dependent on the input parameters of the model such as the heat capacity, thermal conductivity, gas velocity, and the particle radius. The input parameters and case study description can be found in the model definition in Chapter 4.

5.1.1 Temperature Profiles

Figure 5.1 depicts the temperatures in the fluid domain and at the particle surface as a function of the bed height. The lines in the graphs represent the different times of the simulation according to the legend on the right side of the graph. The distance along the sintering bed is represented by the values along the y-axes with the top of the bed at $0.6\,m$ and the bottom at the origin. Gas flow is indicated by the arrows at the left graph and was assumed in the negative y-direction. Comparison of the two profiles shows no significant difference between the temperature in the fluid domain and the particle surface temperature.

As it is not possible to recognize any difference between the two profiles it my be worthwhile to have a closer look at the gas temperature distribution in the left graph of Figure 5.1. At $t = 25\,s$ the gas has already cooled down from $1300\,K$ to approximately $800\,K$ and continues to decrease significantly during the next three time steps (until $t = 200\,s$). After the initial fast cool down the temperature is still decreasing significantly but

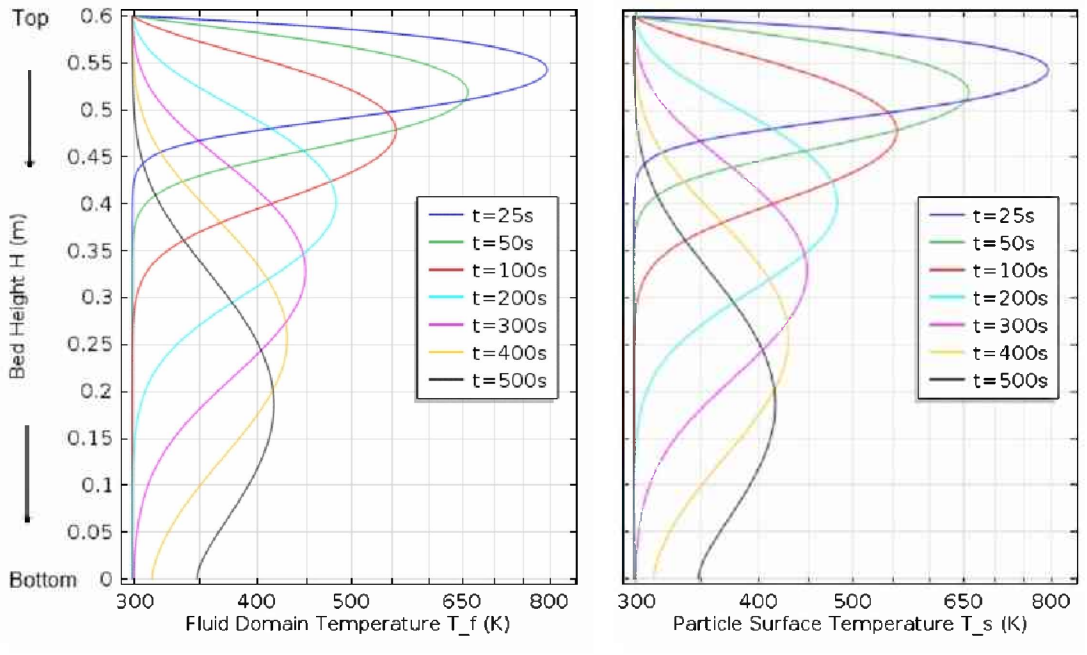

Figure 5.1: Heat transfer case study - Gas temperature in the fluid domain (left), and particle surface temperature in the solid domain (right).

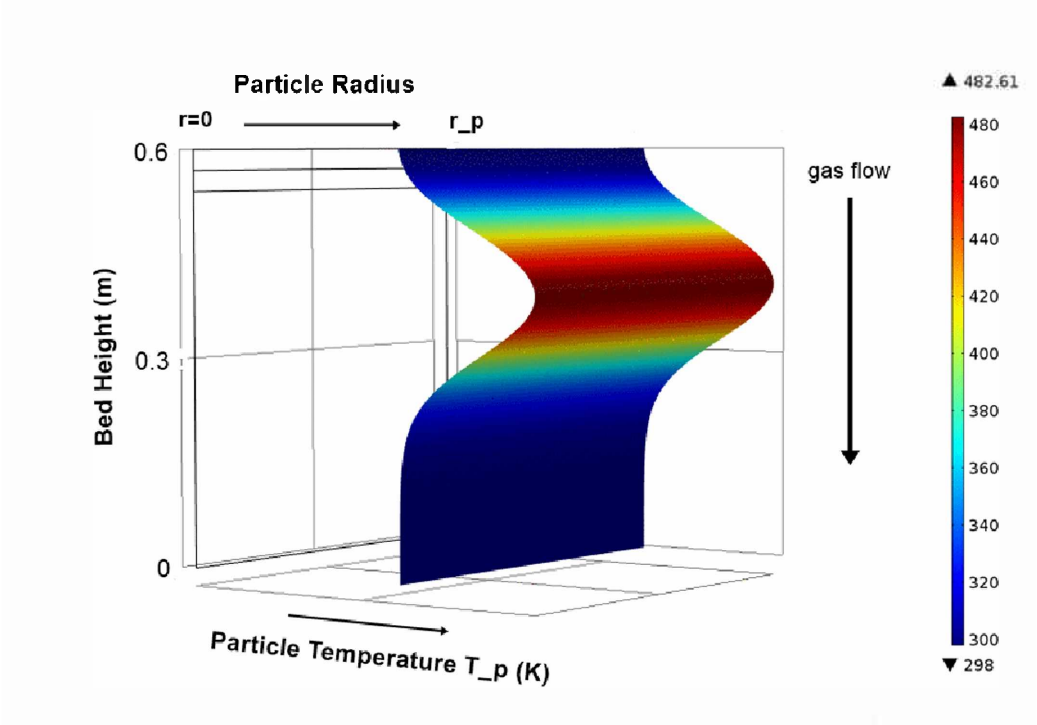

Figure 5.2: Heat transfer case study - 3-D temperature profile in the solid domain, at $t = 200\,\mathrm{s}$.

at a seemingly slower rate. Along with the cooling of the gas goes a broadening of the temperature profile. It looks as if the total area under the curve stays the same during the whole simulation which makes sense from a mathematical point of view. The conservation of energy ensures that as long as the temperature of the outgoing gas is the same as the temperature of the incoming gas ($298\,K$) the amount of energy in the system is constant, and only the temperature distribution in the bed changes. This is the case until $400\,s$ when the temperature at the outlet has already started to increase slightly.

The temperature distribution in the two-dimensional solid domain can be represented as a three-dimensional plot, where the vertical coordinate represents the distance along the bed, and the other two represent the radial coordinate of the particle and the solid temperature T_p respectively (cf. Fig. 5.2). The plot shows the temperature distribution at $200\,s$. The temperature distribution along the particle radius is uniform which implies that the whole particle at a certain point in the bed is heated up uniformly. Temperature uniformity of the particle is caused by the conductivity of the particle, which was set as a material parameter, and also the particle radius. The temperature distribution in Figure 5.2 can be seen exemplary for all other time steps and is also in accordance with the particle surface temperature and the fluid domain temperature distribution in Figure 5.1.

5.1.2 Discussion

The temperature profiles of the case study describe some of the key characteristics of the heat transfer as they have been described in the previous chapters quite well. A travelling heat front as it has been described by Loo [2] can be observed at different times in the temperature profiles of the fluid phase and the particle surface (cf. Fig. 5.1). With advanced time the temperature decreases and the profiles become more and more diffuse.

The broadening of the temperature profiles along with the diminishing temperatures in the bed make it clear that without additional heat from the reactions in the sintering bed the bed temperatures will ultimately drop to the incoming gas temperature of $298\,K$. The broadening temperature profiles however already indicate the trailing end of the characteristic temperature profile (cf. Fig. 2.4).

Another finding from this case study is that the heat is successfully transferred from the solid to the fluid domain and vice versa. In the fluid domain it is transferred mainly by the means of convection as the gas enters the domain at a certain velocity. The cooler solid domain in the lower parts of the bed is heated up by the interfacial heat transfer between the hot fluid and the surface of the particle. Inside the particle conduction leads to a uniform temperature along the particle radius.

With the current configuration no temperature differences within the particles could be observed. Moreover the time that it takes for the heat front to travel to the end of the bed is quite short compared to the timespan of the real sintering process. Some of the encountered issues have been addressed in the next case study which models mass transfer and the chemical reactions in the gas phase of the sintering process.

5.2 Results of the Mass Transfer in the Sintering Bed Case Study

In this case study the mass transfer and chemical reactions have been implemented into the model of the sintering bed. Mass transfer is facilitated by convection and molecular diffusion. The considered reactions are the homogeneous oxidation of carbon monoxide by oxygen and the water gas shift reaction. The reaction rate expressions have been implemented into the model and a stationary study that results in a concentration profile of the chemical species in the bed has been carried out. In contrast to the real sintering process where the reactants of the homogeneous reactions are the product of the preceding combustion reaction in the particles, the chemical species enter the bed with the gas at the inlet of the fluid domain. To study the influence of temperature on the reactions the simulation has been carried out at three different temperatures. The resulting concentration profiles are the subject of the following sections.

5.2.1 Concentration Profiles

5.2.1.1 Fluid Domain Concentration

The concentration profiles for constant gas temperatures of 773, 1273 and 1773 K have been plotted in COMSOL and are presented in Figure 5.3. Compared to the previous case study the bed height represented on the vertical axes has been set from 0.6 to 0.3 m. The direction of the gas flow is indicated by the arrows on the left side of the graph. The concentration can be read from the horizontal axes.

A quick glance at the concentration values on the y-axes already indicates that there are some differences between the profiles obtained at the different temperatures. The absolute values of the concentrations decrease with increasing temperatures. Apart from the magnitude also the shapes of the profiles change with respect to temperature. The specifics of the profiles at the different temperatures will be studied by looking at each profile separately.

Figure 5.4 shows the concentration profile in the upper 10 cm of the bed at 773 K. A steady state is already reached at 0.26 m, only 4 cm after the inlet. The CO_2 and H_2 concentration profiles are identical, therefore not distinguishable from one another, and

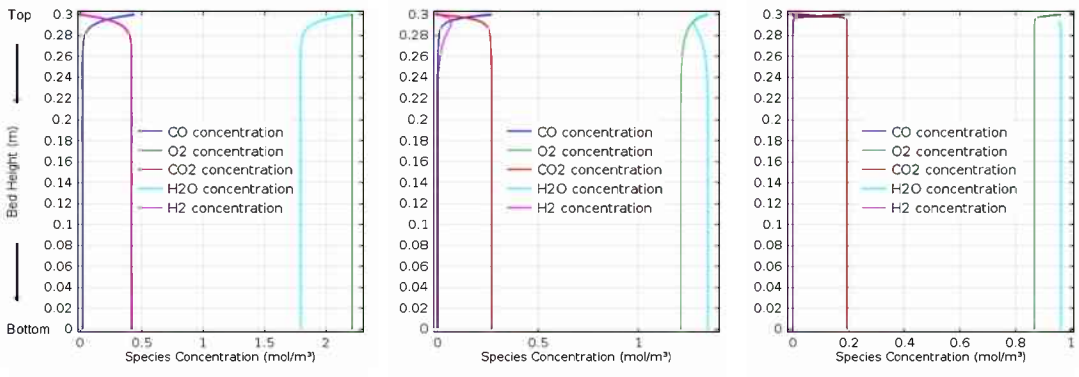

Figure 5.3: Mass transfer case study - Overview of the concentration profiles of the chemical species in the fluid domain at $773\,K$ (left), $1273\,K$ (middle) and $1773\,K$ (right).

increasing from zero at the inlet to about $0.4\,mol/m^3$ at steady state. CO and H_2O values are decreasing while O_2 stays constant in the bed.

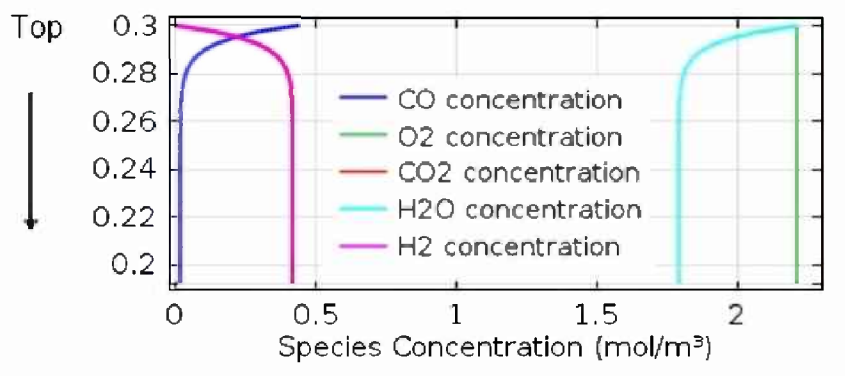

Figure 5.4: Mass transfer case study - Concentration profile of the chemical species in the fluid domain at $773\,K$.

The concentration profile at $1273\,K$ is shown in Figure 5.5. At the beginning the hydrogen concentration in the bed increases, but shortly afterwards decreases again and goes towards zero. The H_2O concentration seems to behave in the opposite way as it decreasing at the top of the bed and soon returns to its initial value close to $1.4\,mol/m^3$. Carbon monoxide shows similar behaviour as at lower temperatures only converging faster towards zero and the carbon dioxide concentration goes up reaching a value of about $0.3\,mol/m^3$. Oxygen concentration decreases at a slower rate than the other species to a steady state value of about $1.2\,mol/m^3$.

Steady state is attained much faster at a temperature of $1773\,K$ (cf. Fig. 5.6). Hydrogen and carbon dioxide concentrations are identical so that their profiles are overlapping.

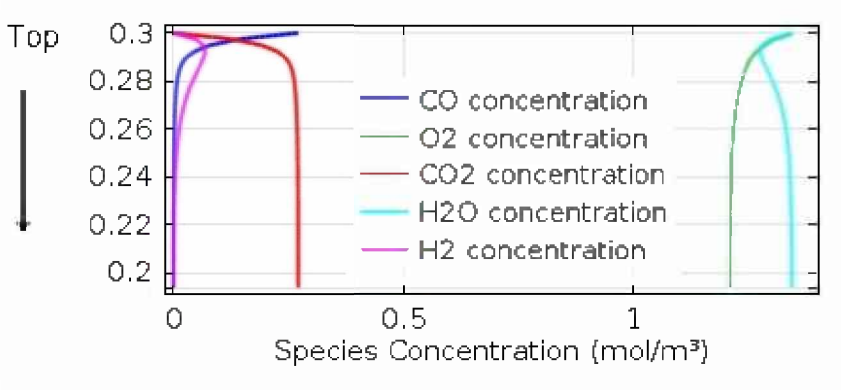

Figure 5.5: Mass transfer case study - Concentration profile of the chemical species in the fluid domain at $1273\,K$.

Their concentrations increase immediately after entering the bed and stay at $0.2\,mol/m^3$. H_2O concentration stays at its initial value of $0.96\,mol/m^3$ while oxygen decreases to about $0.87\,mol/m^3$ and carbon monoxide decreases until it is zero shortly after entering the sintering bed at the top.

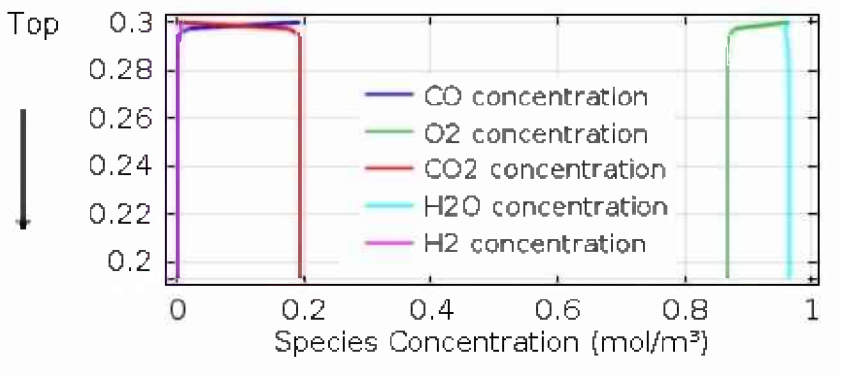

Figure 5.6: Mass transfer case study - Concentration profile of the chemical species in the fluid domain at $1773\,K$.

5.2.1.2 Solid Domain Concentration

The concentration profiles in the 2-dimensional solid domain are plotted as 3-dimensional graphs where the vertical axes is the species concentration and the other two dimensions are the distance along the bed and the particle radius. Figures 5.7 to 5.9 show three exemplary concentration profiles of the chemical species in the solid domain.

The profile in Figure 5.7 shows the carbon monoxide concentration at $773\,K$. At the top of the bed at the particle surface where y equals r_p is the maximum concentration at

$0.2949\,mol/m^3$. Only little amounts of CO enter the particles and only close to the the inlet a concentration gradient can be identified.

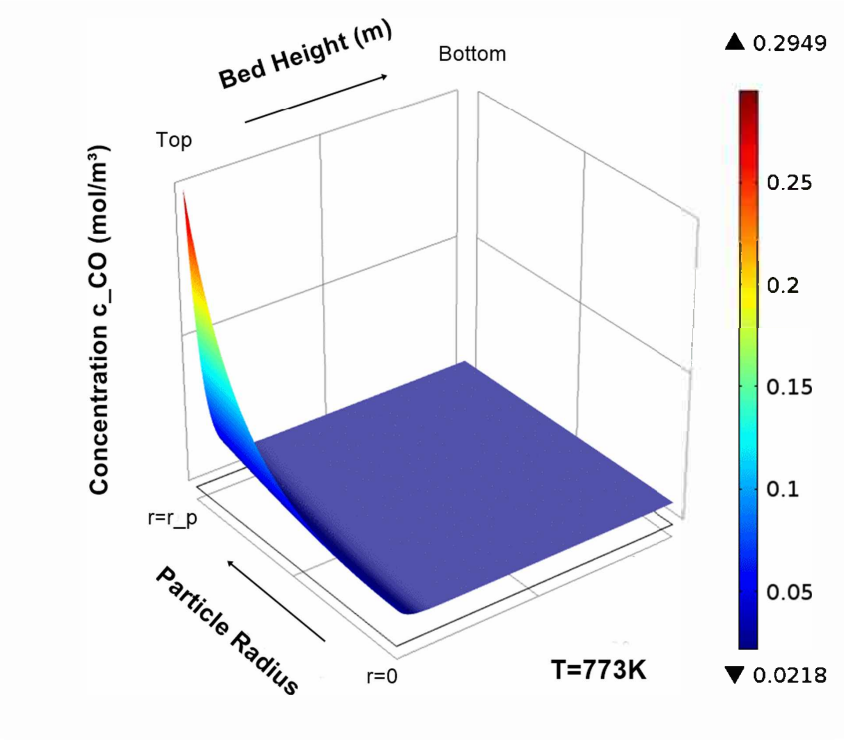

Figure 5.7: Mass transfer case study - CO concentration in the solid domain at $773\,K$.

The 3-dimensional concentration profile of carbon dioxide at $773\,K$ is shown in Figure 5.8. The CO_2 concentration in the solid particles increases rapidly from zero to $0.4214\,mol/m^3$ close to the top of the bed and then stays at a uniform distribution.

The same behaviour as in the fluid domain can be observed for the hydrogen concentration at $1273\,K$ in the solid domain (cf. Fig. 5.9). In the upper part of the bed the H_2 concentration in the particles rises to $0.0669\,mol/m^3$ but shortly after drops to zero again.

5.2.2 Discussion

From the concentration profiles in both domains it is possible to estimate which of the governing chemical reactions is preferred at the specific temperature. Obviously both oxidation reactions have in common a decrease in the carbon monoxide concentration at the expense of the oxygen concentration in Reaction 2.13 and at the expense of water vapour in Reaction 2.14 (cf. Chapter 2). Carbon dioxide is the result of both oxidation reactions accounting for an increase in the CO_2 concentration. The remaining species show differ-

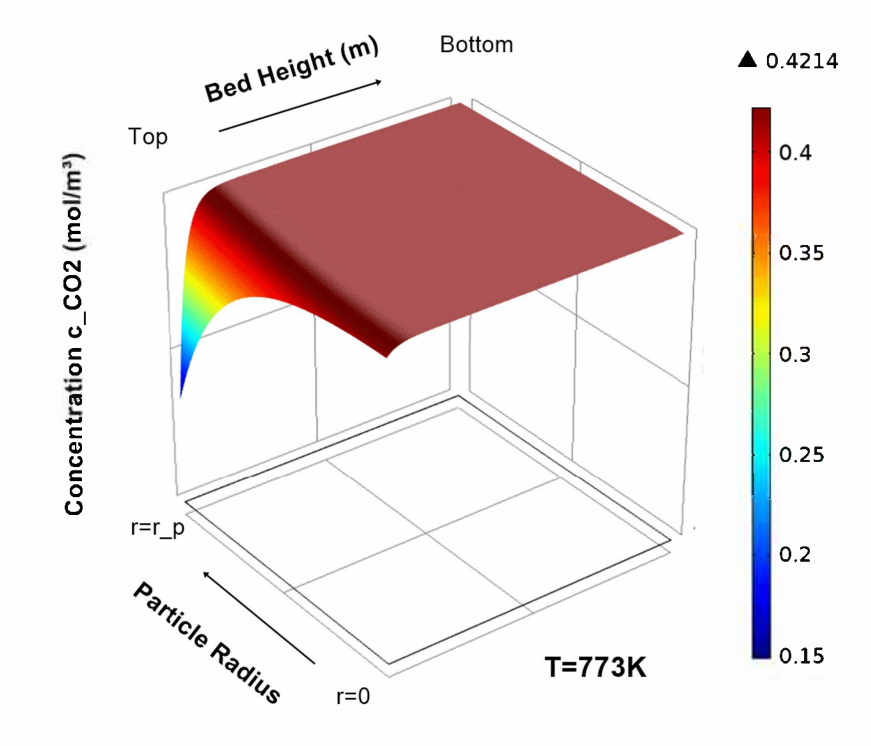

Figure 5.8: Mass transfer case study - CO2 concentration in the solid domain at $773\,K$.

ent concentration profiles depending on the temperature at which the simulation has been carried out.

At $773\,K$ the oxygen concentration stays constant and the concentration of water decreases, which indicates that the water gas shift reaction is the preferred reaction at this temperature. Both the carbon dioxide and the hydrogen concentration are zero at the inlet of the fluid domain and then increase at the same rate and magnitude. This can be explained by the stoichiometry of the water gas shift reaction where for each mole of carbon monoxide that is oxidised, one mole of carbon dioxide and one mole of hydrogen are created. The species taking part in the shift reaction are all subject to the same reaction rate expression which leads to resembling curves in the concentration profile.

The profiles of the chemical species at $1273\,K$ indicate that to a certain degree both oxidation reaction take place in the sintering bed. The curves of hydrogen and water vapour can be explained by the kinetics of the water gas shift reaction, which is an equilibrium reaction. The reaction rate expression in Equation 5.1 shows that the reaction changes its direction once the product of the CO_2 and H_2 concentrations divided by equilibrium constant K_{eq} exceeds the product of the CO and H_2O concentrations. This happens at the turnaround point of the hydrogen and water concentration when the hydrogen concentration

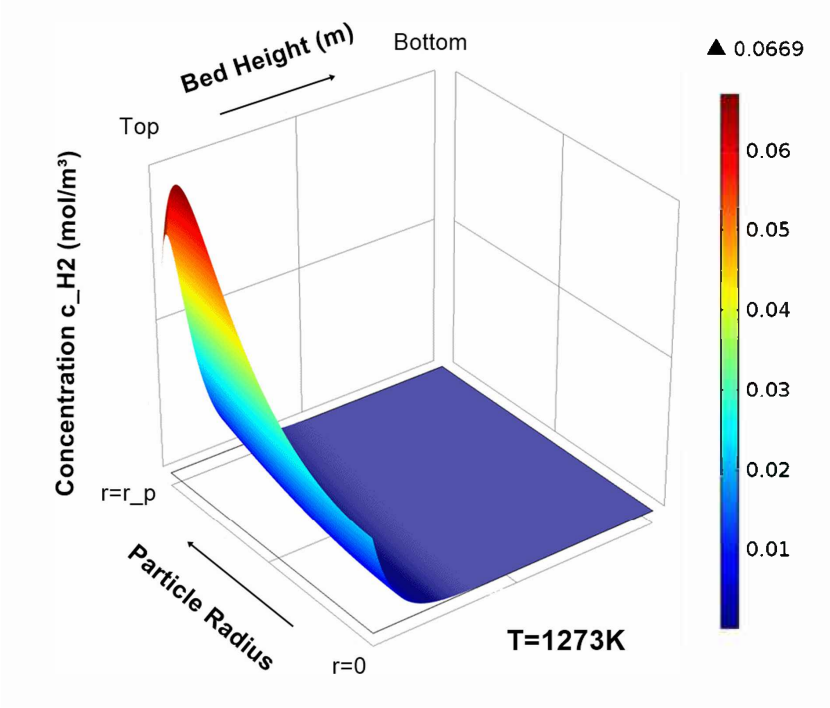

Figure 5.9: Mass transfer case study - Hydrogen concentration in the solid domain at $1273\,K$.

decreases and the water concentration increases again.

$$R_{react,3} = k_{CO,2}\,(c_{CO}\;c_{H_2O} - \frac{c_{CO_2}c_{H_2}}{K_{eq}}) \tag{5.1}$$

The decreasing oxygen concentration beginning at the start of the simulation is an indicator that carbon monoxide is also oxidised by O_2. It can be concluded that at $1273\,K$ under the given concentrations both reactions are taking place in the bed.

The concentration profile at $1773\,K$ indicates that the preferred reaction at this temperature is the carbon monoxide oxidation with oxygen. The oxygen concentration decreases rapidly after entering the bed and the hydrogen and water vapour concentration stay at their initial values. As predicted by the stoichiometry of the oxygen oxidation O_2 and CO concentrations in the plot are decreasing simultaneously. For each oxidized mole of carbon monoxide 0.5 moles of oxygen are consumed by the reaction.

By comparing the three profiles at different temperatures certain trends that go along with rising temperatures can be seen. For once total gas concentration values are decreasing as the temperature increases. This can be explained by the decreasing density of the gas that goes along with higher temperatures, as described by the ideal gas law. The decreased density leads to smaller total concentrations in the gas.

As suggested by the reaction rate expressions in Chapter 2 an increase in the reaction rates goes along with rising temperatures. This can be seen in Figure 5.3 where the concentration gradients are steeper at higher temperatures.

The concentration profiles of the solid domain are in accordance with the fluid domain concentrations. As in the previous case study the values at the particle surface match those of the fluid domain. This is an indicator that the mass transfer coefficient $\beta\,[m/s]$ that has been calculated for the simulation is high enough to enable fast and efficient mass transfer from the fluid to the solid domain (cf. Tab. 5.1).

T	$773\,K$	$1273\,K$	$1773\,K$
β	$0.70\,m/s$	$0.44\,m/s$	$0.33\,m/s$

Table 5.1: Mass transfer case study - Values of the mass transfer coefficient β at 773, 1273 and $1773\,K$.

The concentration profiles at different temperatures show that the results of the simulation strongly depend on the kinetics of the chemical reactions which are greatly influenced by the temperature in the bed. One of the limiting factors of the reactions is the concentration of carbon monoxide. Constant concentration profiles in the bed are established as soon as all the CO has reacted. That implies no more oxidation reactions can take place. In the sintering process the combustion of coke continuously produces carbon monoxide which leads to more reactions in the lower parts of the bed. Also the additional heat produced by the reaction has an influence on the kinetics and would have to be considered in further studies.

5.3 Results of the Coupling of Heat and Mass Transfer in the Sintering Bed Case Study

This case study combines the previous two models by coupling the chemical reactions to the heat transfer interfaces. The temperature in the bed is no longer constant which impacts the rates of oxidation and the heat and mass transport mechanisms between the two domains. By looking at the heat and concentration profiles the influence on the heat and mass transfer will be studied.

5.3.1 Concentration Profiles

A look at the fluid domain concentration profiles in Figure 5.10 shows no significant difference compared to the mass transfer case study (cf. Fig. 5.3).

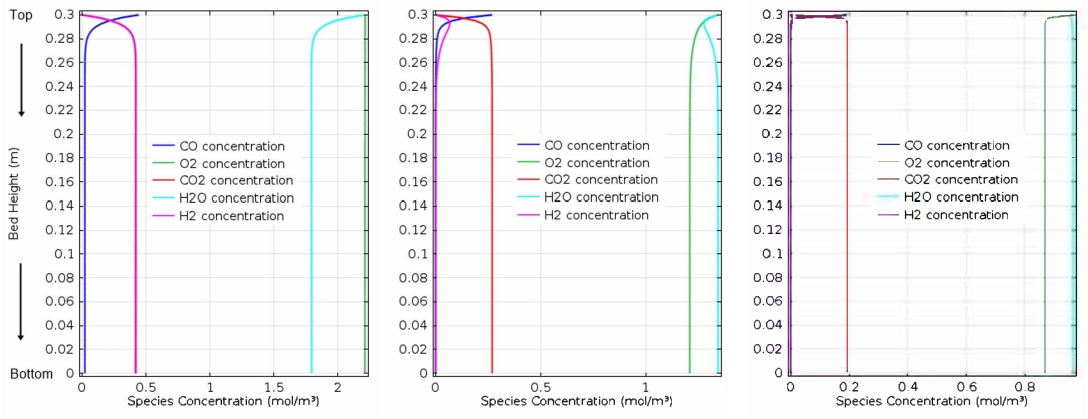

Figure 5.10: Heat and mass transfer case study - Overview of the concentration profiles of the chemical species in the fluid domain at $773\,K$ (left), $1273\,K$ (middle) and $1773\,K$ (right).

A look at the concentration profiles in the solid domain leads to the same conclusion. The plots in Figure 5.11 show the same profiles that have already been illustrated in the results section of the mass transfer case study.

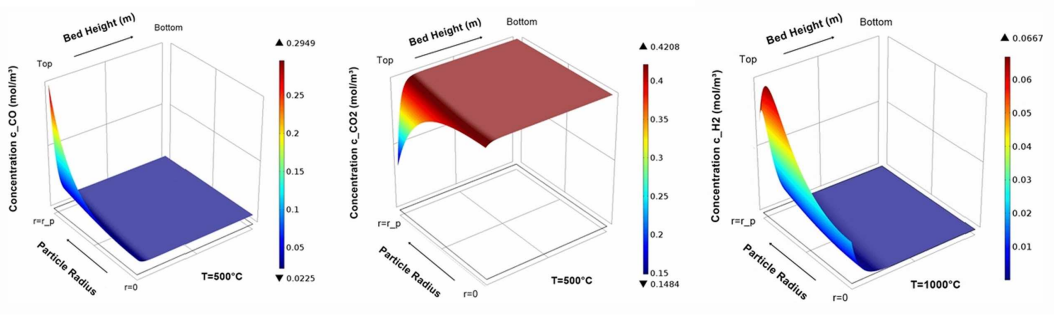

Figure 5.11: Heat and mass transfer case study - Concentration profiles of the chemical species in the solid domain (L-R: CO concentration at $773\,K$, CO_2 concentration at $773\,K$, H_2 concentration at $1273\,K$).

5.3.2 Temperature Profiles

A look at the temperature profiles shows the effect of the heat from the chemical reactions on the temperature in the bed. In figure 5.12 the profiles at inlet gas temperatures of 773, 1273 and $1773\,K$ are shown. Increasing temperatures along the bed height can be observed in all three graphs.

At an inlet temperature of $773\,K$ a temperature increase can be observed until the gas

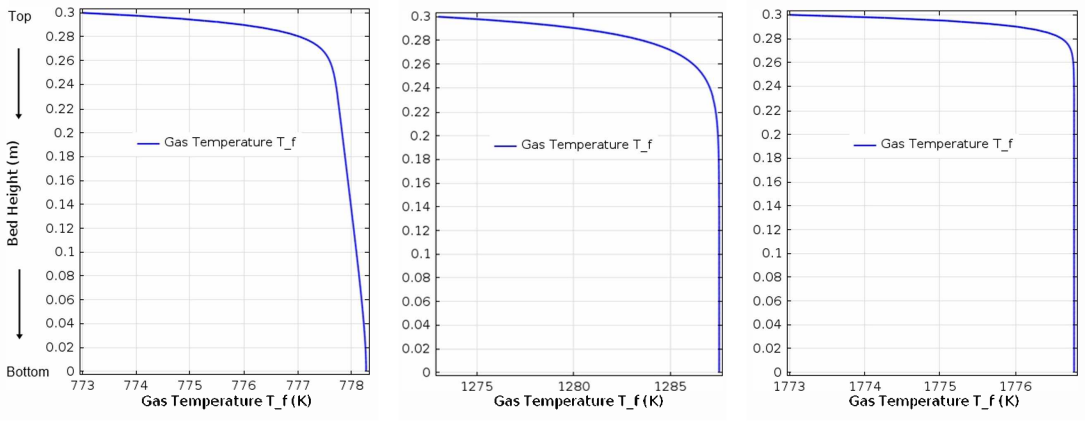

Figure 5.12: Heat and mass transfer case study - Temperature profiles in the fluid domain at inlet temperatures of 773, 1273 and 1773 K.

leaves the bed. The total temperature increase is 7 K. The temperature difference between in and outgoing gas at 1273 K is approximately 12 K. A difference of only a little less than 4 K at 1773 K makes the second profile the one with the highest temperature increase. The calculated temperatures at the bottom of the bed are presented in Table 5.2.

T_{in}	773 K	1273 K	1773 K
T_{out}	778.3 K	1287.5 K	1776.8 K

Table 5.2: Heat and mass transfer case study - Temperature values at in and outlet of the sintering bed.

5.3.3 Discussion

An effect of the temperature increase on the chemical reactions could not be observed in the concentration profiles above. However, the case study shows, due to the temperature increase in the bed, that the coupling of the heat and mass transfer is principally working. A possible explanation for the small effect is that the main heat contributor in the sintering process, the combustion reaction of coke, was not considered in the case study so that an important heat source is missing. Also the concentration values at the inlet might have been too small to lead to a bigger change in temperature. Nevertheless, the temperature profiles show that heat is generated by the reactions and is transported within the bed.

5.4 Results of the Heterogeneous Reaction Case Study

In the surface reaction case study the laminar flow field has been calculated in a stationary study and then used in the calculation of the heat and mass transport. Figure 5.13 shows the velocity distribution in the flow cell. The velocity of the gas is higher between the spheres where the the space is limited and it is lower close to the surface of the spheres and the surface of the walls respectively. The maximum velocity in the cell is at $0.2155\,m/s$, showing a considerable increase from the inlet velocity of $0.08\,m/s$.

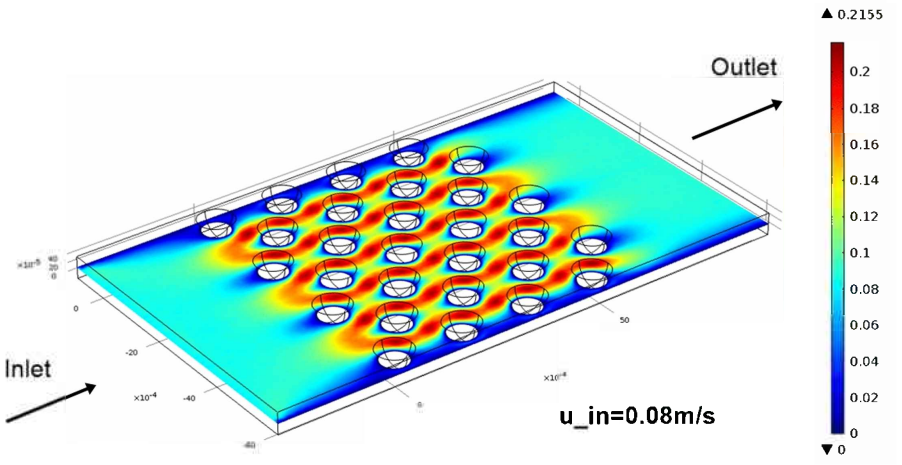

Figure 5.13: Heterogeneous reaction case study - Velocity profile in the flow cell.

5.4.1 Concentration Profiles

Figures 5.14 and 5.15 show the fluid phase concentrations of oxygen and carbon monoxide at 0.01, 0.04 and $0.08\,s$. Oxygen enters the flow cell at $t = 0\,s$ at a concentration of $1.3621\,mol/m^3$. The concentration profile at $t = 0.08\,s$ is slightly curved with lagging concentrations at the side walls of the cell.

Carbon monoxide is the reaction product in the cell and is created as soon as oxygen reaches the surface of a particle. At $t = 0.01\,s$ a CO concentration peak can already be observed at the front spheres in the flow cell. The creation of carbon monoxide is analogous to the movement of oxygen in Fig. 5.14 and shows the same curved profile, seen most strikingly at $t = 0.08\,s$. The CO concentration is highest at the surfaces of the spheres and the maximum concentration of $0.3762\,mol/m^3$ can be observed in the last shown time step.

Figures 5.16 and 5.17 show the surface coverage of carbon (C) and its surface fraction with respect to time. The development of the surface coverage is quite similar to the

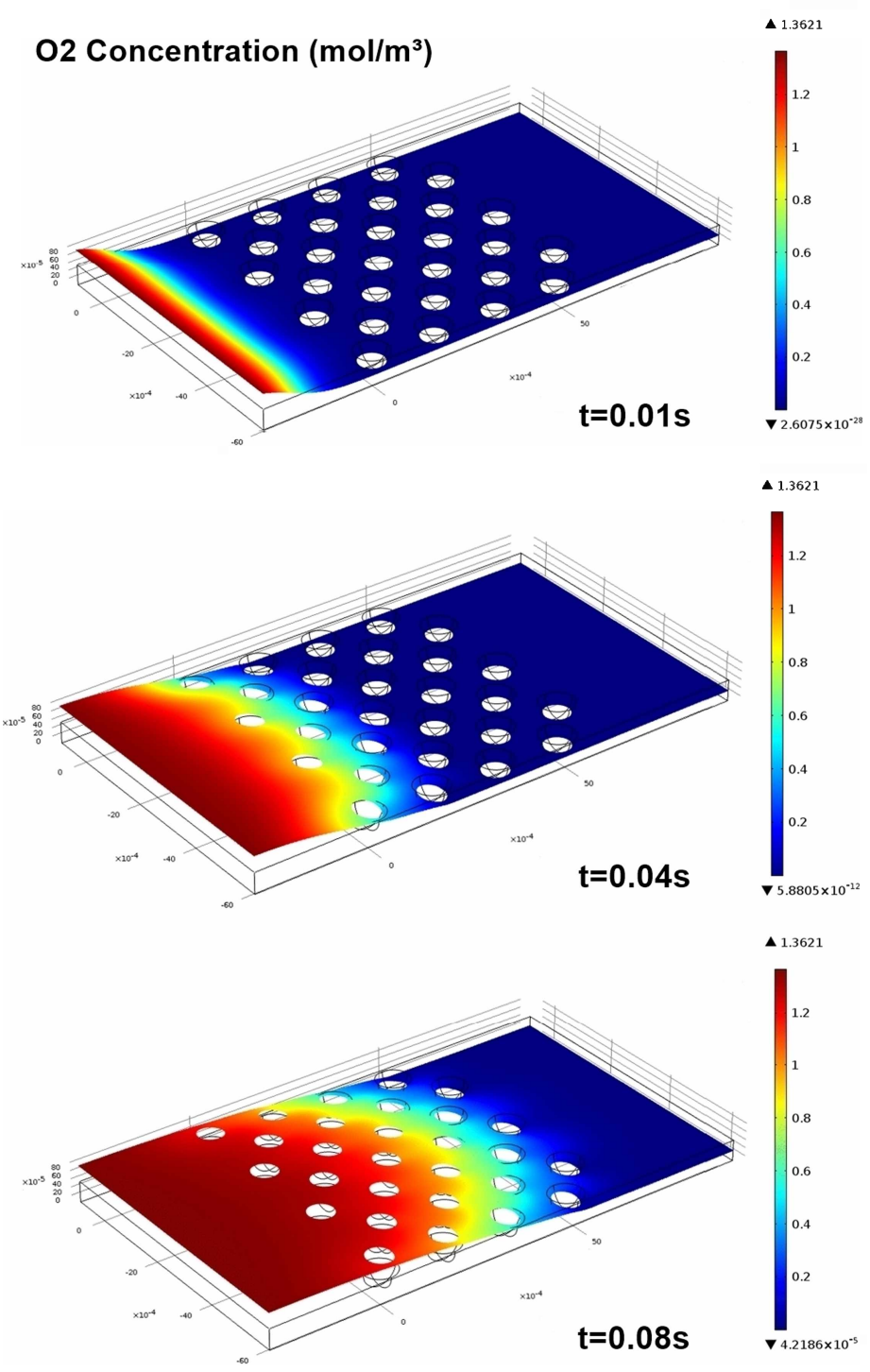

Figure 5.14: Heterogeneous reaction case study - Oxygen concentration $[mol/m^3]$ in the flow cell at 0.01, 0.04 and 0.08 s.

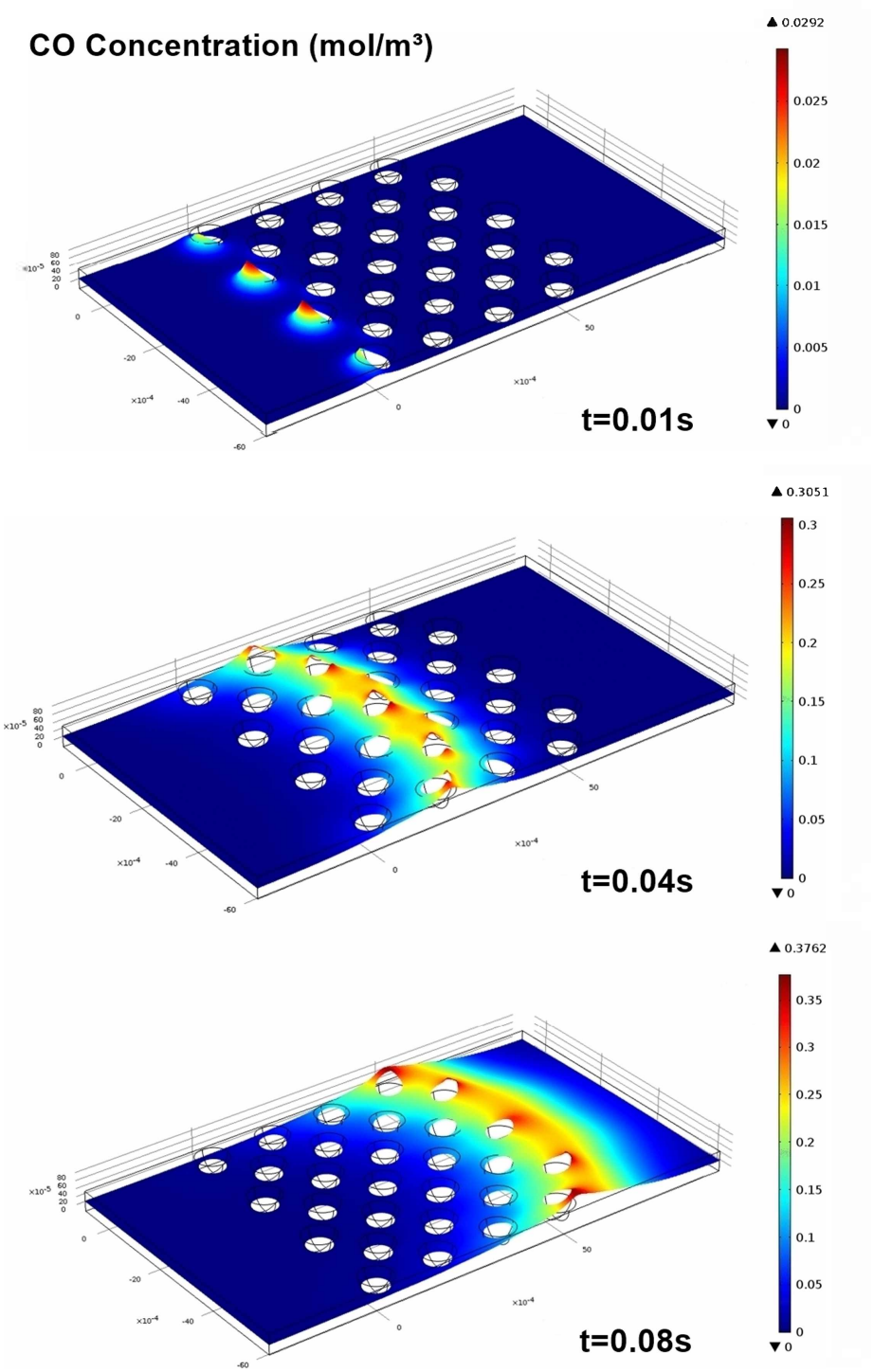

Figure 5.15: Heterogeneous reaction case study - Carbon monoxide concentration $[mol/m^3]$ in the flow cell at 0.01, 0.04 and 0.08 s.

concentration profiles of oxygen and carbon monoxide. At $0.01\,s$ only the front spheres shows decreased surface coverage and only at their front faces. At $0.04\,s$ about half of the carbon in the bed has reacted and at $0.08\,s$ barely any carbon is left in the bed.

The development of the surface fraction on the first and last of the centred spheres with respect to time is shown in Figure 5.17. The decrease of Carbon is linear and the time gap between the front and back spheres in the cell is approximately $0.05\,s$.

5.4.2 Temperature Profiles

The temperature profiles in Fig. 5.18 show the changing temperatures in the bed due to chemical reactions taking place at the particle surfaces. The initial temperature in the bed is $1300\,K$. At $0.01\,s$ the temperature starts to rise at the spheres in the front. In the subsequent time steps the temperature continues to rise in the successive spheres and the temperature profile in the bed gets broader, reaching a maximum temperature at $0.08\,s$ of $1328.4\,K$.

5.4.3 Discussion

The concentration and temperature profiles along with surface fraction show a consistent image of the species movement and reactions in the flow cell. The representation of the velocity distribution in the bed shows the acceleration of the fluid when the cross section of the cell decreases. The maximum velocity in the cell is more than 2.6 times as fast as the inlet velocity of $0.08\,m/s$. The no slip boundary condition manifests itself in a velocity of zero on the solid surfaces of the walls and spheres in the cell.

The concentration profiles of oxygen and carbon monoxide in the fluid phase are coupled to the velocity profile and show the characteristic curve for a flow in a contained volume due to its resistance to flow at the sides of the wall. The profiles at $0.08\,s$ strongly resemble the parabolic profile of a laminar flow in a pipe. From the carbon monoxide profiles in Figure 5.15 it is discernible that at $0.01\,s$ some of the oxygen already reaches the front row of spheres where it immediately reacts with the carbon on the surface. The surface concentration of carbon drops to zero within $0.02\,s$ after the the oxygen reaches the particle. This can be explained by the fast reaction rates at these temperatures but also by the comparably low surface concentration of carbon.

Heat is created at the surface were the reactions take place leading to hot spots at the spheres in the bed. The temperature travels along the bed simultaneously to the development of the concentration profiles in Figures 5.14 through 5.16. With time the temperature profile in the bed gets broader. Once the oxygen has passed the last spheres all the carbon on the surface has reacted and no more heat is produced. The reactions in

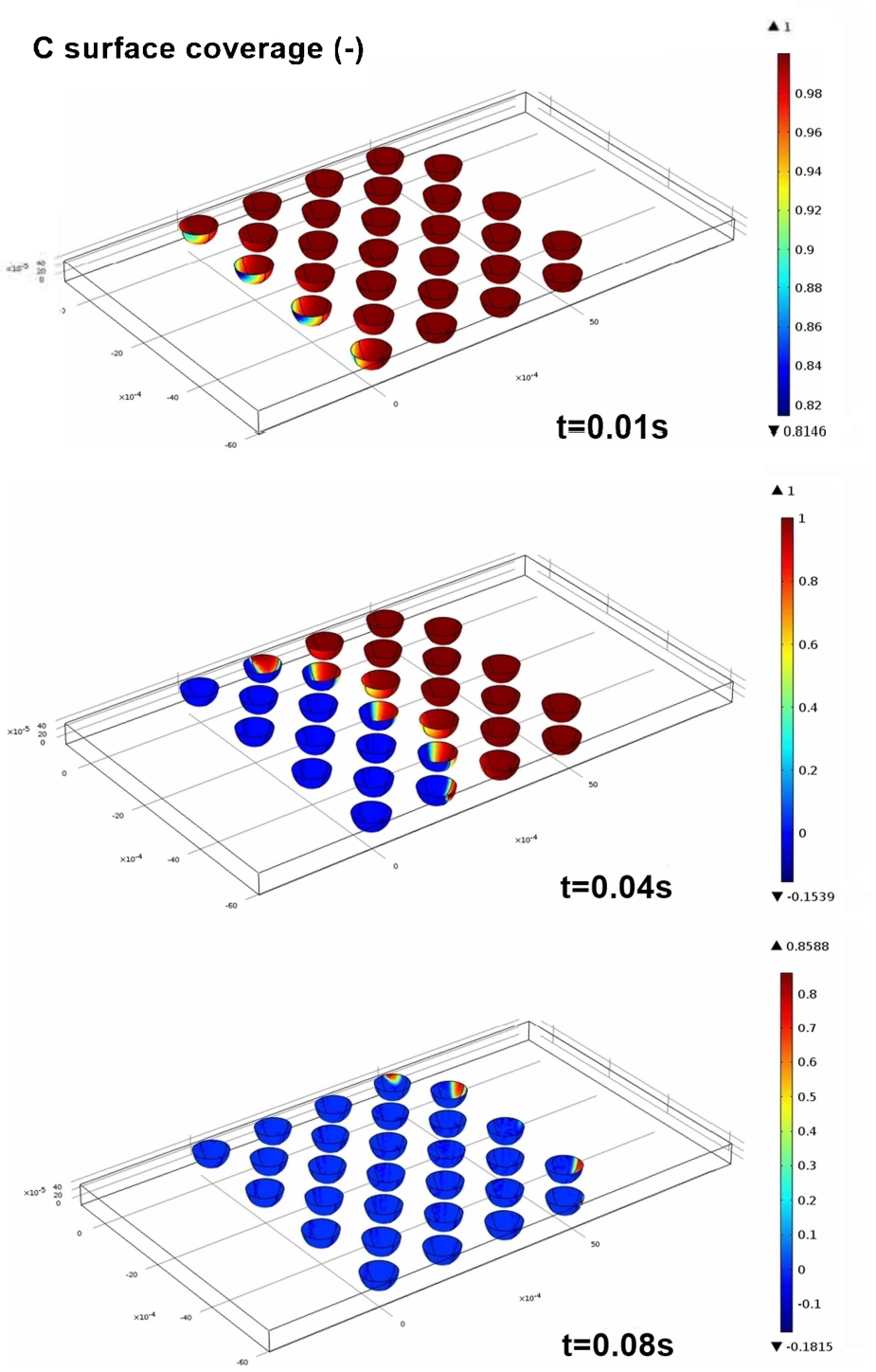

Figure 5.16: Heterogeneous reaction case study - Carbon surface coverage [-] in the flow cell at 0.01, 0.04 and 0.08 s.

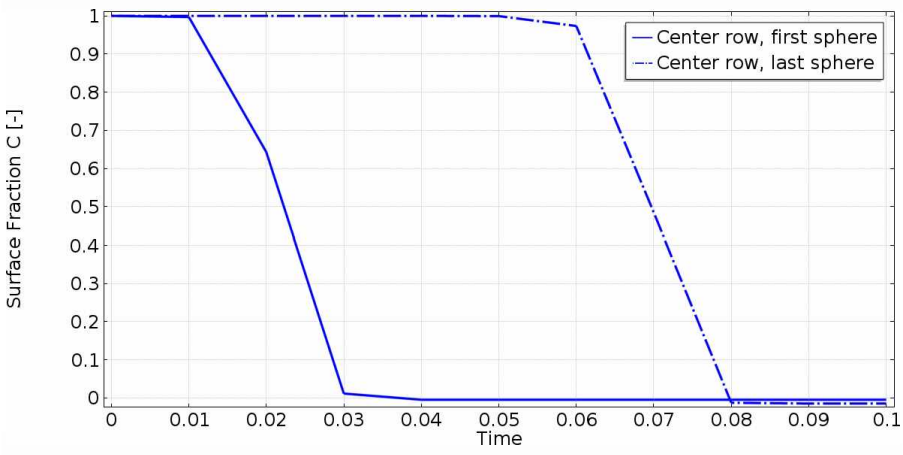

Figure 5.17: Heterogeneous reaction case study - Carbon surface fraction [-] with respect to the time t on the first and last spheres in the center row.

the bed will automatically come to an end and the temperature will resume to its initial temperature of $1300\,K$.

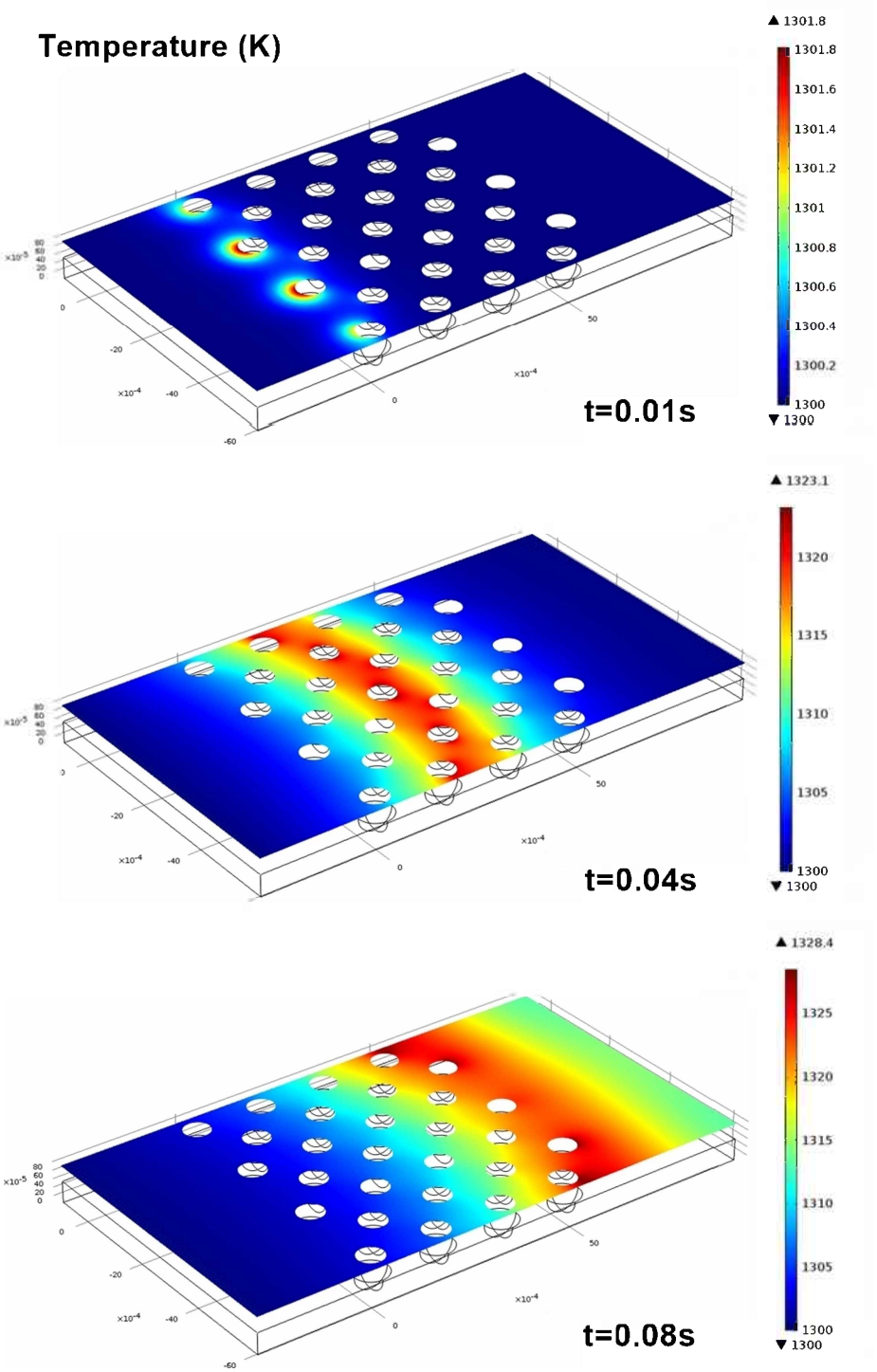

Figure 5.18: Heterogeneous reaction case study - Temperatures in the flow cell at 0.01, 0.04 and 0.08 s.

Chapter 6

Summary and Conclusions

The goal of this work was to model heat and mass transfer mechanisms of the iron ore sintering process using the finite element software COMSOL Multiphysics®. The used approach was to model case studies that treat processes like the mass and heat transfer or the chemical reactions in a packed bed made of spheres, similar to the geometry of the bed in the sintering process. A basic description of the sintering bed, the theory behind the heat and mass transfer mechanisms, the implementation into the software and four case studies that have been conducted plus their results are the content of this work.

The first three case studies used similar geometry and modelling assumptions in order to describe the heat and mass transfer in the sintering bed. A so called multigeometry approach as well as a number of adaptations to account for the spherical shape of the particles were implemented into the case studies. The made assumptions along with its implications are described in Chapters 2 and 3. The set up of the COMSOL case studies and the resulting temperature and concentration profiles are in the Chapters 4 and 5.

The first case study treats the heat transfer in the sintering bed. Material parameters and process conditions that are similar to the conditions in the actual sintering process have been applied to the model, e.g. a temperature of $1300\,K$ had been applied to the upper part of the geometry which represents the hot cover layer of the sintering bed after ignition. The results show the characteristic development of the heat front, which travels downwards in the bed until it leaves the modelling domain.

Along with the mass transport in the bed two chemical reactions that take place in the gas phase during iron ore sintering were modelled in the second case study. The considered reactions were the oxidation of carbon monoxide with oxygen and the water gas shift reaction. The reactants enter the bed with the gas at the bed inlet and diffuse into the particles where the reactions take place. During the whole simulation the temperatures in the bed and the concentrations of the chemical species at the inlet of the geometry were held at a constant value. In order to study the influence of the temperature on the chemical

reactions the simulation had been carried out at 773, 1273 and 1773 K. At 773 K the water gas shift reaction is the preferred reaction route and at 1773 K the oxidation with oxygen. Both reactions are taking place simultaneously in the case study at 1273 K.

A combination of the first two case studies was modelled in the third case study of this thesis. The model contains heat and mass transfer interfaces for the solid and the fluid domain and couples their variables in order to calculate the temperature and chemical species distributions in the sintering bed. The temperature is coupled to the chemical reaction rates and the heat of the reactions is implemented as a source term in the heat transfer interface. Again, the study had been carried out at gas inlet temperatures of 773, 1273 and 1773 K. Differences in the concentration profiles were minimal and only little increase in temperature along the bed could be observed.

The fourth and last case study represents an approach for modelling the heterogeneous combustion reaction of coke with oxygen as a surface reaction on the particles in the sintering bed. The model was set up in a flow cell that contains a set of spheres where the oxygen containing gas passes through and reacts with the carbon on the surface of the spheres. The flow field has been modelled as a laminar flow and the resulting velocity distribution is the base for modelling the heat and mass transport in the bed. The resulting concentration profiles show the species concentrations of oxygen and of the reaction product carbon monoxide. The surface coverage and surface fraction of carbon at different times of the simulation could also be attained from the simulation. The combustion reaction releases heat which could be observed in the temperature profile of the flow cell. The calculation ends after all the carbon on the surface has reacted and no more chemical reactions are taking place in the bed.

6.1 Conclusions

This thesis presents methods to study the heat and mass transfer in a packed bed with COMSOL Multiphysics®. The specific case studies in this thesis applied different approaches to study the heat and mass transfer as well as the homogeneous and heterogeneous chemical reactions in the sintering bed. The first three case studies used a multigeometry approach to describe the processes in the sintering bed. In the fourth case study the heterogeneous reaction was modelled as a surface reaction in a three-dimensional flow cell.

The multigeometry approach reduces the complex geometry of the bed to a 1-D fluid domain and a 2-D solid domain. This requires less computational power and leads to reduced calculation times. The number of mesh elements of the first three case studies is 240 for the fluid domain geometry and 3600 for the geometry of the solid domain model. The number of mesh elements in the 3-D geometry of the heterogeneous reaction case study is with

more than 130,000 elements comparatively high. Regarding these numbers the difference in calculation time, a couple of minutes compared to two or more hours is not surprising.

From a theoretical standpoint the outcome of the simulations, the temperature and concentration distributions in the bed, is in concordance with existing theory and the observable trends can be explained by theoretical considerations and the principle set up of the models. Starting with this basic study of the characteristics of the sintering process further studies need to be conducted in order to set up more advanced models of the process and achieve better understanding of the prevailing conditions in the bed.

Future studies should aim to model heat and mass transfer, homogeneous and heterogeneous reactions into one comprehensive sintering model. To achieve this the principles of the heterogeneous surface reaction case study should be implemented into a case study that uses the multigeometry approach of case studies 1 to 3. The great strength of this approach is the ability to solve coupled systems of partial differential equations encompassing complicated reaction terms, with comparably little computational resources.

In case study 4, the heterogeneous reaction model, the mass transport of oxygen to the particle surface and the diffusion into the particle to the reaction interface have not been considered. A possible approach is to model the heterogeneous reaction by introducing additional terms into the surface reaction rate expression. Further review of existing publications on the topic of heterogeneous reaction modelling and multiphysics applications could give valuable input for new approaches and ideas.

In addition experimental tests and comparison with available literature in order to validate the simulation should be considered in future investigations. To achieve better results the quality of the input parameters of a simulation is crucial. Investing time and resources in order to attain a consistent and thorough description of the process conditions and parameters is definitely worth the effort and will be rewarded by achieving better results.

A sound model of the heat transfer processes and a proper understanding of the governing mechanisms is important for further investigations into bed permeability, pressure loss and other factors that affect sintering productivity and sinter quality. Adding more reactions to the model provides future opportunities to attain better knowledge of the amount and nature of the gaseous emissions and possible environmental impact of the sinter production process.

Bibliography

[1] J. Strassburger, *Blast Furnace-theory and Practice.* No. v. 1 in Blast Furnace, Gordon and Breach Science Publishers, 1969.

[2] C. E. Loo, "Changes in heat transfer when sintering porous goethitic iron ores," *Mineral Processing and Extractive Metallurgy*, vol. 109, no. 1, pp. 11–22, 2000.

[3] C. E. Loo and J. C. M. Leaney, "Characterizing the contribution of the high-temperature zone to iron ore sinter bed permeability," *Mineral Processing and Extractive Metallurgy*, vol. 111, no. 1, pp. 11–17, 2002.

[4] C. E. Loo and J. Aboutanios, "Changes in water distribution when sintering porous goethitic iron ores," *Mineral Processing and Extractive Metallurgy*, vol. 109, no. 1, pp. 23–35, 2000.

[5] V. Wolf, "Skriptum zu Chemische Technologien - Metallurgie," 2012. Montanuniversität Leoben - Institut für Verfahrenstechnik des industriellen Umweltschutzes.

[6] K. Taube, *Stahlerzeugung Kompakt.* Vieweg Technik, Vieweg, 1998.

[7] E. UK, "Simplified diagram of a sintering plant." `http://www.eurotherm.co.uk/en-gb/industries/heat-treatment/metals-applications/sintering`, April 2014.

[8] C. E. Loo, "A perspective of goethitic ore sintering fundamentals," *ISIJ International*, vol. 45, no. 4, pp. 436–448, 2005.

[9] C. Weiß, "Skriptum zu Stoffbilanzen und Stoffeigenschaften," 2010. Montanuniversität Leoben - Institut für Verfahrenstechnik des industriellen Umweltschutzes.

[10] R. Polke, M. Schäfer, and N. Scholz, *Charakterisierung disperser Systeme: Abschnitt 2.2*, pp. 45–75. Wiley-VCH Verlag GmbH & Co. KGaA, 2005.

[11] R. Polke, M. Schäfer, and N. Scholz, *Charakterisierung disperser Systeme: Abschnitt 2.1*, pp. 7–45. Wiley-VCH Verlag GmbH & Co. KGaA, 2005.

[12] S. Ergun and A. A. Orning, "Fluid flow through randomly packed columns and fluidized beds," *Industrial & Engineering Chemistry*, vol. 41, no. 6, pp. 1179–1184, 1949.

[13] J. H. Ferziger and M. Perić, *Numerische Strömungsmechanik.* Springer London, Limited, 2008.

[14] K. Hertwig and L. Martens, *Chemische Verfahrenstechnik: Berechnung, Auslegung und Betrieb chemischer Reaktoren.* Oldenbourg Wissenschaftsverlag, 2011.

[15] H. Baehr and K. Stephan, *Wärme- und Stoffübertragung.* Springer Berlin Heidelberg, 2013.

[16] M. Drozd and C. Weiß, "Forschungsbericht: Koksgrusoberflächenreaktionen und NOx-Bildungsmechanismen beim Sinterprozess," tech. rep., Institut für Verfahrenstechnik des industriellen Umweltschutzes, Montanuniversität Leoben, 2010.

[17] C. Malek, *Zur Bildung von Stickstoffoxid bei einer Staubfeuerung unter gleichzeitiger Berücksichtigung des Ausbrandes.* CUTEC-Schriftenreihe; Nr. 6, Culliver Verlag, Göttingen, 1 ed., 1993. Dissertation TU Clausthal.

[18] J. Mitterlehner, *Modeling and Simulaton of Heat Front Propagation in the Iron Ore Sintering Process.* PhD thesis, Vienna University of Technology, 2002.

[19] R. C. Reid, J. M. Prausnitz, and T. K. Sherwood, *The properties of gases and liquids.* McGraw-Hill chemical engineering series, McGraw-Hill, 1977.

[20] L. D. Smoot and P. J. Smith, *Coal Combustion and Gasification.* The Plenum Chemical Engineering Series, Springer, 1985.

[21] J. B. Howard, G. C. Williams, and D. H. Fine, "Kinetics of carbon monoxide oxidation in postflame gases," *Symposium (International) on Combustion*, vol. 14, no. 10, pp. 975–986, 1973. Fourteenth Symposium (International) on Combustion.

[22] J. Kotz, P. Treichel, and J. Townsend, *Chemistry and Chemical Reactivity, Enhanced Edition*, ch. 5.7, p. 233. Available 2010 Titles Enhanced Web Assign Series, Cengage Learning, 7 ed., 2009.

[23] M. L. de Souza-Santos, *Solid Fuels Combustion and Gasification: Modeling, Simulation, and Equipment Operations.* Dekker Mechanical Engineering, Taylor & Francis, 2004.

[24] R. J. B. Smith, L. Muruganandam, and S. S. Murthy, "A review of the water gas shift reaction kinetics," *International Journal of Chemical Reactor Engineering*, vol. 8, 2010.

[25] R. R. Lovel, K. R. Vining, and M. Dell'amico, "The influence of fuel reactivity on iron ore sintering," *ISIJ International*, vol. 49, no. 2, pp. 195–202, 2009.

[26] F. Allain and A. G. Dixon, "Modeling of transport and reaction in a catalytic bed using a catalyst particle model," in *Proceedings of the COMSOL Conference 2010 Boston*, 2010.

[27] COMSOL Multiphysics®, *Packed Bed Reactor Tutorial*, 2013. Solved with COMSOL Multiphysics 4.3b.

[28] COMSOL Multiphysics®, *Spherically Symmetric Transport Tutorial*, 2012. Solved with COMSOL Multiphysics 4.3.

[29] COMSOL Multiphysics®, *COMSOL Multiphysics User's Guide, Version 4.3*, May 2012. Solved with COMSOL Multiphysics 4.3b.

[30] COMSOL Multiphysics®, *Surface Reactions in a Biosensor Tutorial*, 2013. Solved with COMSOL Multiphysics 4.3b.

[31] P. A. Nikrityuk, M. Gräbner, M. Kestel, and B. Meyer, "Numerical study of the influence of heterogeneous kinetics on the carbon consumption by oxidation of a single coal particle," *Fuel*, vol. 114, pp. 88 – 98, 2013.

List of Figures

List of Tables

Abbreviations and Symbols

Abbreviations

Abbreviation	Description
1-D	One-dimensional
2-D	Two-dimensional
3-D	Three-dimensional
BC	Boundary condition
cf.	Confer (Latin), means compare
C	Carbon
Chap.	Chapter
CO	Carbon monoxide
CO_2	Carbon dioxide
COMSOL	COMSOL Multiphysics®
CT	Computer tomography
°C	Degree celsius
e.g.	Exempli gratia (Latin), means for example
Eq.	Equation
Fig.	Figure
grad	Gradient
H_2	Hydrogen
H_2O	Water
i.e.	Id est (Latin), means that is
in	Ingoing
IC	Initial condition
L-R	Left to right
N_2	Nitrogen
O_2	Oxygen
PDE	Partial differential equation
®	Registered trademark
SMD	Sauter mean diameter
Tab.	Table
WGSR	Water gas shift reaction

Symbols and Units

Latin Letters

Symbol	Description	Unit
A	Area	m^2
A_p	Specific particle surface area	m^2/m^3
c	Concentration	mol/m^3
c_p	Specific molar (isobaric) heat capacity	J/(molK)
d_a	General Form PDE damping coefficient	
d	Diameter	m
D	Diffusion coefficient	m^2/s
D_e	Effective diffusion coefficient	m^2/s
e_a	General Form PDE mass coefficient	
f	General Form PDE source term	
g	General Form PDE interface boundary flux	
Ea	Activation energy	J/mol
h	Specific molar enthalpy	J/mol
H	Bed height	m
H_r	Reaction enthalpy	J/mol
$\mathbf{I}$	3x3 identity matrix in Navier Stokes equation	
k_{eff}	Effective reaction resistance	m/s
k_i	Kinetic frequency factor	cf. Eq. 2.5.2, Eq. 2.5.2
k_s	Kinetic constant	$s\,Pa\,m^{-1}$=$s\,kg\,m^{-3}$
K_{eq}	Equilibrium constant	-
M	Molar weight	g/mol
n	Number of molecules	mol
$\vec{n}$	Normal vector	-
p	Pressure	Pa; bar
p_i	Partial pressure of species i	Pa
Δp	Pressure difference	Pa
Q	Convective heat source	W/m^3
$\dot{q}$	Heat flux density	W/m^2
R	Universal gas constant	$J/(mol\,K)$
R_i	Reaction rate source term	$mol/(m^3\,s)$
$R_{s,i}$	Surface reaction rate source term	$mol/(m^2\,s)$
R_{react}	Reaction rate expression	$mol/(m^3\,s)$
$R_{s,react}$	Surface reaction rate expression	$mol/(m^2\,s)$
r	Spherical particle coordinate	m
$\hat{r}$	Dimensionless particle radius	-
r_c	Reacting core radius	m
$\dot{S}$	Source term in the general conservation equation	-
t	Time	s
t_0	Starting time	s
T	Absolute temperature	K
u	Velocity	m/s

Greek Letters

Symbol	Description	Unit
α	Heat transfer coefficient	$\mathrm{W/(m^2\,K)}$
β	Mass transfer coefficient	$\mathrm{m/s}$
ϵ	Emissivity	-
ε	Porosity	-
η	Dynamic viscosity	$\mathrm{kg/(ms)}$
Γ	Flux vector; Conservative flux	-
λ	Thermal conductivity	$\mathrm{W/(m\,K)}$
ν	Kinematic viscosity	$\mathrm{m^2/s}$
ν_i	Stoichiometric coefficient	-
ϕ	Variable in the general conservation equation	-
$\dot{S}_\phi$	Conservation equation source term	-
φ	space angle in the spherical coordinate system	°
σ	Stefan-Boltzmann constant	$\mathrm{W/(m^2\,K^4)}$
$\sigma_{c_s,i}$	Site occupancy number	-
ρ	Density	$\mathrm{kg/m^3}$
τ	Tortuosity	-
θ	space angle in the spherical coordinate system	°

Indices

Indices	Description
0	At $t = 0\,s$
b	Bed
$bulk$	Bulk temperature, concentration, etc.
f	Fluid phase
i	Chemical species i
j	Chemical reaction j
in	Ingoing
out	Outgoing
p	Particle, i.e. solid phase
s	Particle surface
t	Transport
tot	Total
x	Cartesian coordinate x
y	Cartesian coordinate y

Units

Symbol	Unit	Quantity
$bar = 10^5 Pa$	Bar	Pressure
J	Joule	Energy; Quantity of heat
$J/(kgK)$	Joule per kilogram kelvin	Specific heat capacity
$J/(m^3 s)$	Watt per cubic metre	Heat source
$K = 273.15 + °C$	Kelvin	Temperature
kg	Kilogram	Mass
$kg/m3$	Kilogram per cubic metre	Density
kJ	Kilojoule	Energy; Quantity of heat
m	Metre	Length
m^2	Square metre	Area
m^2/s	Square metre per second	Kinematic viscosity
m^3	Cubic metre	Volume
$mm = 10^{-3}\,\mathrm{m}$	Millimetre	Length
$\mu m = 10^{-6}\,\mathrm{m}$	Micrometre	Length
mol	Mole	Amount of substance
mol/m^3	Mole per cubic metre	Concentration
m/s	Metres per second	Velocity
$Pa = N/m^2$	Pascal	Pressure
Pas	Pascal second	Dynamic viscosity
s	Second	Time
$W = J/s$	Watt	Power; Heat flux
W/m^2	Watt per square metre	Heat flux density
W/m^3	Watt per cubic metre	Heat source

Calculations

Equations of the Case Studies

Heat Transfer in the Sintering Bed Case Study

Heat Transfer Case Study - Heat Transfer in Fluids Interface

Heat Transfer in Fluids $$\rho_f \cdot c_{p,f} \cdot \frac{\partial T_f}{\partial t} + \rho_f \cdot c_{p,f} \cdot u_{x,f} \cdot \frac{\partial T_f}{\partial x} = \frac{\partial}{\partial x} \cdot (\lambda_f \cdot \frac{\partial T_f}{\partial x}) + Q_f$$
Heat Source $$Q_f = A_p \cdot \alpha \cdot (T_s - T_f)$$

Heat Transfer Case Study - General Form PDE Interface

General Form PDE $$e_a \cdot \frac{\partial^2 T_p}{\partial t^2} + d_a \cdot \frac{\partial T_p}{\partial t} + \nabla \Gamma = f$$
Damping or Mass Coefficient $$d_a = y^2 \cdot \rho_p \cdot c_{p,p}$$
Conservative FLux in the y-direction $$\Gamma_y = -\lambda_p \cdot \frac{y^2}{r_p^2} \cdot \frac{\partial T_p}{\partial y}$$
Boundary Flux/Source $$g = \frac{y^2}{r_p} \cdot \alpha \cdot (T_{bulk} - T_s)$$

Heat Transfer Case Study - Parameters and Variables

$$\rho_f = \frac{p_{atm} \cdot M_g}{R \cdot T_f}$$

$$\lambda_f = 0.3056 \cdot T_f^{0.7821}$$

$$u_x = u_{in} \cdot \frac{T_f}{273K \cdot \varepsilon_b}$$

$$\eta_f = -1 \cdot 10^{-11} \cdot T_f^2 + 5 \cdot 10^{-8} \cdot T_f + 3 \cdot 10^{-6}$$

Heat Transfer Case Study - Physics Model Coupling

Fluid Domain Variable $$T_s = mod2.genext2(mod2.T_p)$$
Solid Domain Variable $$T_{bulk} = mod1.genext1(mod1.T_f)$$

Mass Transfer in the Sintering Bed Case Study

Mass Transfer Case Study - Transport of Diluted Species Interface

Transport of Diluted Species $$u_{x,f} \cdot \frac{\partial}{\partial x} \cdot c_{i,f} = D_i \cdot \frac{\partial^2 c_i}{\partial x^2} + R_{i,f}$$
Reactions source term $$R_{i,f} = -A_p \cdot c_{i,flux}$$
Species flux $$c_{i,flux} = D_i \cdot \frac{y}{r_p} \cdot \frac{\partial c_{i,s}}{\partial y}$$

Mass Transfer Case Study - General Form PDE Interface

General Form PDE $$e_a \cdot \frac{\partial^2 T_p}{\partial t^2} + d_a \cdot \frac{\partial T_p}{\partial t} + \nabla \Gamma = f$$
Damping coefficient $$d_a = y^2 \cdot \rho_p \cdot c_{p,p}$$
Conservativ flux in the y-direction $$\Gamma_y = -\lambda_p \cdot \frac{y^2}{r_p^2} \cdot \frac{\partial T_p}{\partial y}$$
Source term $$f_i = y^2 \cdot \sum_j (\nu_{i,j} \cdot R_j)$$
Boundary flux/source $$g = \frac{y^2}{r_p} \cdot \beta \cdot (c_{i,bulk} - c_{i,p})$$

Mass Transfer Case Study - Reaction Rates for the Homogeneous Reactions

Homogeneous gas phase reactions

$$\mathrm{CO(g)} + \tfrac{1}{2}\,\mathrm{O_2(g)} \longrightarrow \mathrm{CO_2(g)}$$
$$\mathrm{CO(g)} + \mathrm{H_2O(g)} \longleftrightarrow \mathrm{CO_2(g)} + \mathrm{H_2(g)}$$

CO oxidation with oxygen

$$R_{react,2} = k_2 \cdot \exp(-\frac{Ea_2}{R \cdot T_f}) \cdot c_{CO} \cdot c_{O_2}^{\frac{1}{2}} \cdot c_{H_2O}^{\frac{1}{2}}\ [\frac{mol}{m^3 s}]$$
$$k_2 = 1.3 \cdot 10^8\ [\frac{(m^3)^3}{mol^2 s}]$$
$$Ea_2 = 125604\ [\frac{J}{mol}]$$

Water gas shift reaction

$$R_{react,3} = k_3 \cdot (c_{CO} \cdot c_{H_2O} - \frac{c_{CO_2} \cdot c_{H_2}}{K_{eq}})\ [\frac{kmol}{m^3 s}]$$
$$k_3 = 2.78 \cdot 10^3 \cdot \exp(-\frac{1510}{T_f})\ [\frac{m^3}{kmol s}]$$
$$K_{eq} = 0.0265 \cdot \exp(\frac{3968}{T_f})\ [-]$$

Mass Transfer Case Study - Parameters and Variables

$$D_f(T_f) = D_f(T_{ref}) \cdot (\frac{T_{ref}}{T_f})^{\frac{3}{2}}$$

$$c_{in,i} = c_{in,tot} \cdot x_{in,i}$$

$$c_{in,tot} = \frac{p_{atm}}{R \cdot T_{in}}$$

Mass Transfer Case Study - Physics Model Coupling

Fluid Domain Variable

$$c_{i,flux} = mod2.genext2[D_i \cdot \frac{y}{r_p} \cdot \frac{\partial(mod2.c_i)}{\partial y}]$$

Solid Domain Variable

$$c_{i,bulk} = mod1.genext1(mod1.c_i)$$

Coupling of the Heat and Mass Transfer in the Sintering Bed Case Study

The case study uses the same interfaces as the heat transfer case study and the mass transfer case study. The set up of the interfaces is identical to the set up in the previous studies. Only the *General Form PDE* for the Heat Transfer has an additional *Heat Source* node.

Heat and Mass Transfer Case Study - General Form PDE Interface (Heat Transfer)

Heat Source

$$f = -y^2 \cdot (R_{react2} \cdot H_{r,2} + R_{react3} \cdot H_{r,3})$$

Heterogeneous Surface Reaction Case Study

Heterogeneous Reaction Case Study - Laminar Flow Interface

Laminar Flow

$$\rho_f \mathbf{u} \cdot \nabla \mathbf{u} = \nabla [-p\mathbf{I} + \eta_f (\nabla \mathbf{u} + (\nabla \mathbf{u})^T) - \frac{2}{3} \eta_f (\nabla \cdot \mathbf{u}) \mathbf{I}]$$
$$\nabla \cdot (\rho_f \mathbf{u}) = 0$$

Heterogeneous Reaction Case Study - Transport of Diluted Species Interface

Transport of Diluted Species

$$\frac{\partial c_i}{\partial t} + \nabla \cdot (-D_i \nabla c_i) + \mathbf{u} \cdot \nabla c_i = 0$$

Heterogeneous Reaction Case Study - Surface Reaction Interface

Transport of Diluted Species

$$\frac{\partial c_i}{\partial t} + \nabla_t \cdot (-D_{s,i} \nabla_t c_{s,i}) = R_{s,i}$$

Heterogeneous Reaction Case Study - Heat Transfer in Fluids Interface

Heat Transfer in Fluids

$$\rho_f \cdot c_{p,f} \cdot \frac{\partial T_f}{\partial t} + \rho_f \cdot c_{p,f} \cdot u_{x,f} \cdot \frac{\partial T_f}{\partial x} = \frac{\partial}{\partial x} \cdot (\lambda_f \cdot \frac{\partial T_f}{\partial x}) + Q_f$$

Heat Flux

$$\dot{q} = -H_{react} \cdot R_{react}$$

Heterogeneous Reaction Case Study - Reaction Rates for the Homogeneous Reactions

Heterogeneous combustion reactions $$\mathrm{C(s)} + \tfrac{1}{2}\,\mathrm{O_2(g)} \longrightarrow \mathrm{CO(g)}$$
Reaction Kinetics $$R_{react} = k \cdot c_{O_2} \cdot cshr.theta\_free$$ $$k = 1.692 \cdot T \cdot \exp(-\frac{0.0582 \cdot 10^5}{R \cdot T})$$

Heat Transfer Coefficient Calculations

Calculation of the heat transfer coefficient.

$$\alpha = \frac{\lambda_f}{2\ r_p}\ f_a\ (2 + (Nu_{lam}^2 + Nu_{turb}^2)^{\frac{1}{2}})$$

$$f_a = 1 + 1.5\ (1 - \varepsilon)$$

$$Nu_{lam} = 0.664\ \sqrt{Re_\varepsilon}\ \sqrt[3]{Pr}$$

$$Nu_{turb} = \frac{0.037\ Re_\varepsilon^{0.8}\ Pr}{1 + 2.443\ Re_\varepsilon^{-0.1}\ (Pr^{\frac{2}{3}} - 1)}$$

$$Re_\varepsilon = \frac{\rho_f\ u_f\ d_p}{\mu_f\ \varepsilon}$$

$$Pr = \frac{\mu_f}{\rho_f\ a}$$

$$a = \frac{\lambda_f}{\rho_f\ c_{p,f}}$$

Mass Transfer Coefficient Calculations

Calculation of the mass transfer coefficient.

$$\beta = \frac{D_{e,O_2}}{2\ r_p}\ f_a\ (2 + (Sh_{lam}^2 + Sh_{turb}^2)^{\frac{1}{2}})$$

$$f_a = 1 + 1.5\ (1 - \varepsilon)$$

$$Sh_{lam} = 0.664\ \sqrt{Re_\varepsilon}\ \sqrt[3]{Sc}$$

$$Sh_{turb} = \frac{0.037\ Re_\varepsilon^{0.8}\ Sc}{1 + 2.443\ Re_\varepsilon^{-0.1}\ (Sh^{\frac{2}{3}} - 1)}$$

$$Re_\varepsilon = \frac{\rho_f\ u_f\ d_p}{\mu_f\ \varepsilon}$$

$$Sc = \frac{\mu_f}{\rho_f\ D}$$